國立交通大學

光電工程學系　顯示科技研究所

碩士論文

高分子薄膜電晶體之退火效應

The annealing effect on polymer thin-film transistors

研究生：黃泰元

指導教授：陳方中 博士

中華民國九十六年七月

高分子薄膜電晶體之退火效應

The annealing effect on polymer thin-film transistors

研 究 生：黃泰元　　Student：Tai-Yuan Huang

指導教授：陳方中 博士　　Advisor：Dr. Fang-Chung Chen

國 立 交 通 大 學

電機學院顯示科技研究所碩士班

碩 士 論 文

A Thesis

Submitted to Display Institute

College of Electrical and Computer Engineering

National Chiao Tung University

in partial Fulfillment of the Requirements

for the Degree of

Master

in

Display Institute

July 2007

Hsinchu, Taiwan, Republic of China

中華民國九十六年七月

高分子薄膜電晶體之退火效應

碩士研究生：黃泰元　　指導教授：陳方中

國立交通大學顯示科技研究所碩士班

中文摘要

本論文利用二種熱退火方式：熱退火和溶劑退火來增加以高分子為主動層的薄膜電晶體的元件特性。實驗結果得知，即使沒有在主動層與二氧化矽絕緣層之間加入修飾層，元件的效率仍然可以藉由退火效應而得到提升。比較發現，溶劑退火增加的特性較熱退火明顯。結合二種退火方式，我們能進一步增加元件的整體特性。經過分析，我們認為相較於熱退火，溶劑退火的方式可以大幅改善高分子自我排列的能力，而形成具有較高規則性的薄膜，也因此造成元件特性的改善。

The annealing effect on polymer thin-film transistors

Student : Tai-Yuan Huang **Advisor : Dr. Fang-Chung Chen**

National Chiao Tung University

ABSTRACT

We introduced two annealing methods, thermal annealing and solvent annealing to increase the performance of poly(3-hexylthiophene) thin-film transistors. The done performance was enhanced by the annealing process even without the interface treatment between the insulator and the active layer. Comparing of the two annealing processes, the enhancement of the solvent annealing is more significant. Furthermore, the performance of devices can be increased by combining the two of the annealing processes.

The solvent annealing can assist the self-organization of P3HT rather than the thermal annealing. The self-organization of P3HT would form more regular films and results in the enhancement of P3HT devices.

誌　　謝

在這兩年的碩士研究生涯中，我受到了許多人的幫助，無論是研究內容或是生活態度上的建議，都令我獲益良多，僅以此文獻給我由衷感謝的人。

首先，我要感謝指導教授陳方中博士。在研究生涯當中，老師帶給了我許多課業上的新知識以及實驗中的技巧，使我得以突破研究上的困境。而老師在對我做事情態度上的叮嚀更是深刻的教誨，讓我做實驗的時候能夠事半功倍，相信我學到的內容會成為將來我的生活中不可或缺的一部分。

感謝文奎、祖榮、喬舜、志平學長在這兩年中將自己的經驗及技巧毫不保留地傳授教導，每每都讓我開拓了視界。特別要感謝的是祖榮學長在我實驗上的指點，總是能給在迷霧中的我一條道路而有所依從。在與祖榮學長的討論氣氛也總是輕鬆愉快的，也能吸收許多自己缺乏的知識。

接著要感謝永昇、立仁、東賢、映頻，以及文生、瑞祥、惠君、思芳學長姐的帶領，讓我能在短時間內掌握實驗室的狀況。也感謝你們無私的付出為實驗室建立了良好的環境，無論是實驗設備的完善或是人際關係間的和諧，讓我能夠喜歡這間充滿親切氣氛的實驗室。

陪伴我兩年的伙伴，上傑、義凱、浩偉、志力、紓婷、尹婷，感謝大家在實驗上的配合、努力，以及相互間的扶持協助，讓每個人都得以順利完成自己的研究生涯。還有大家在實驗問題上熱烈的討論、遇到挫折時的勉勵、實驗成功時喜悅的分享，這些所有的點點滴滴都將成為我這段時間的最美麗的回憶。

實驗室的學弟妹，呈祥、昱仁、太獅、曉芬、煒琪、政豪、永軒、信展，有你們的加入，才能使得實驗室有著無數的歡笑，感謝你們處理實驗室的大小事務，讓我能心無旁騖地專心於自己的實驗上頭。特別是呈祥和昱仁在量測上的幫忙，沒有你們的協助，相形之下這篇論文將失色不少，誠摯地感謝你們的辛勞。

最後我要感謝我最親愛的父母以及弟弟，在求學的過程，有你們作為我的支柱，時常的慰問我，以及提供我無憂無慮的環境，才使我得以順利完成學業，這是我最感激的部分，也是我最珍貴的資產。你們的關心是這篇論文完成最大的動力，同時也是我最珍惜的事物。

Contents

List of Table

Figure Captions

Chapter 1

Introduction

1.1 Organic Electronics

The organic electronics have been widely applied to various aspects [1], such as organic light-emitting diodes (OLEDs), organic solar cells, organic thin-film transistors (OTFTs) etc. The advantages are described as followings:

(1) Solution processibility: organics can be solved in organic solvents. The solution can be used in the spin coating, and ink-jet printing to realize the large-area fabrication.

(2) Low-temperature processibility can be used to deposite organic molecules solution processes. The highest temperature of processes occurs in the annealing step, usually from 100 ℃ to 200 ℃. Hence the plastic can be used as the substrate to fabricate the flexible productions.

(3) Light-weight.

The disadvantages of organic electronics are unstable, and lower mobility.

In 1983, F, Ebisawa et al. announced the polyacetylene and polysiloxane to be the active layer and the dielectrics of OTFTs. [2] The electrical transfer characteristics is shown in Fig. 1-1. The field-effect mobility was on the order of 10^{-5} cm^2/Vs. Later, new materials like polythiophene were discovered. [3] However, the mobility was still low. Then The poly(3-hexylthiophene) was used to be the active layer in TFT by A. Assadi et al. in 1988. [4] The pentacene devices has been reported in 1992. [5] The mobility is about $2x10^{-3}$ cm^2/Vs. Recently, the most popular organic materials used in OTFTs is pentacene. Fig. 1-2 shows the evolution of organic thin-film transistors. In 2000, the mobility of pentacene has

surpassed that of the amorphous silicon.

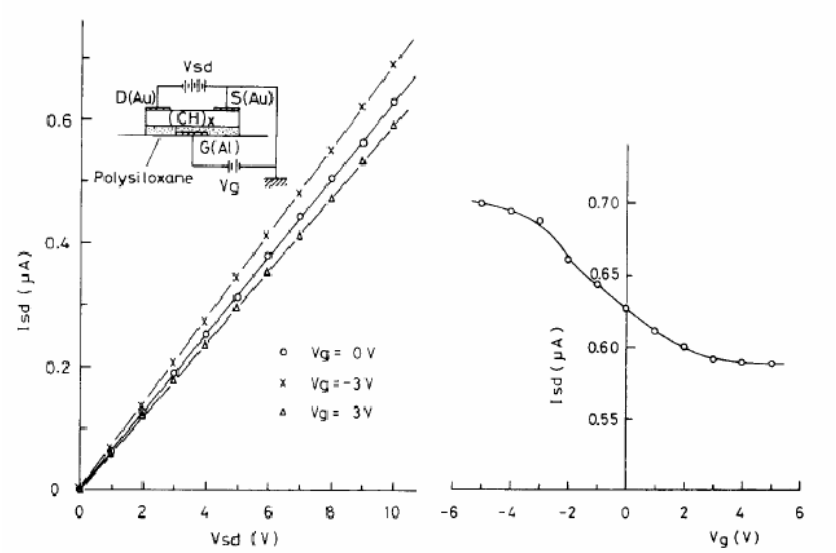

Fig. 1-1 In 1983, the TFT was made by polyacetylene and polysiloxane [2]

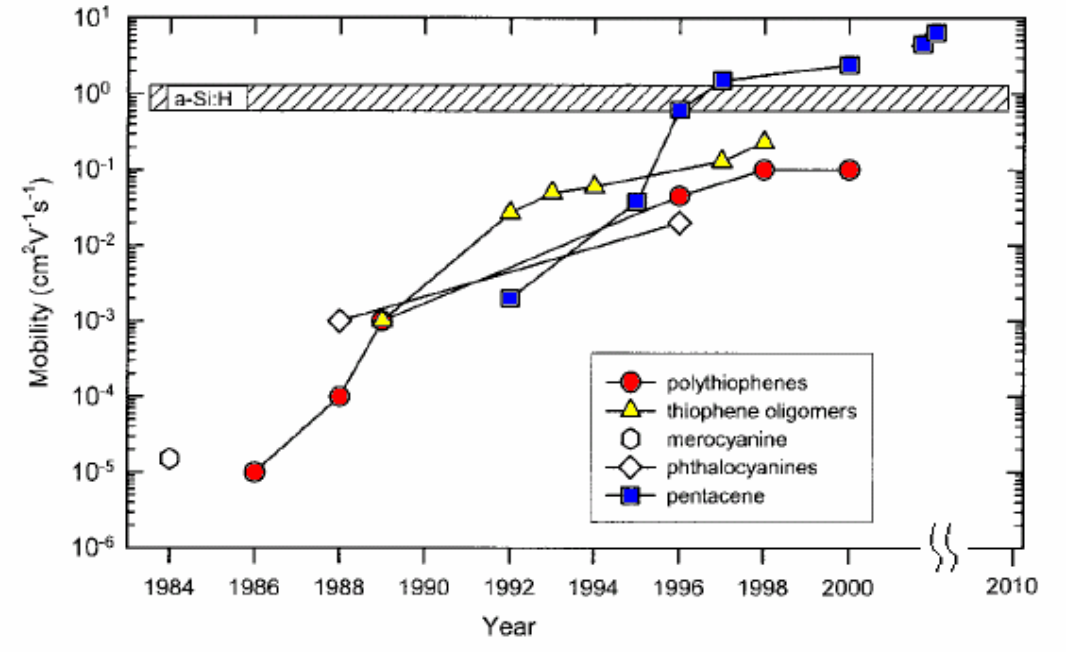

Fig. 1-2 The evolution of organic electronics [6]

1.2 Introduction to the Conjugated Polymer

A system consisting of alternating single bonds and double bonds in polymer is called as conjugated polymers. The polyacetylene is a typical type of conjugated polymer as illustrated in Fig. 1-3. [7] Three of the four valence electrons of carbon form hybridized sp2 orbitals and bind to neighboring atoms with the σ-bond. The one electron that does not form hybridized sp^2 orbitals binds to the neighboring carbon atoms with the π-bond. Owing to the conjugated polymer structure, the charges can transport in polymers by the resonant of π-bounding electrons.

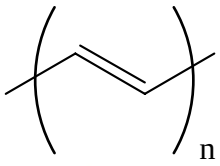

Fig. 1-3 Molecular structure of polyacetylene

1.3 Introduction to the P3HT

Poly(3-hexylthiophene), P3HT, is a conjugate polymer and is used as the active layer of organic thin-film transistors in this article. Four carbon atoms and one sulfur atom compose a thiophene. The thiophene is the main chain structure of the P3HT. The side chain of P3HT is a hexyl group. Depending on the position of the alkyl chain to the main chain, there are two different regioregularities: head-to-tail and head-to-head, respectively. Fig. 1-4 shows the chemical structure of the P3HT and the different structure between the head-to-tail and the head-to-head.

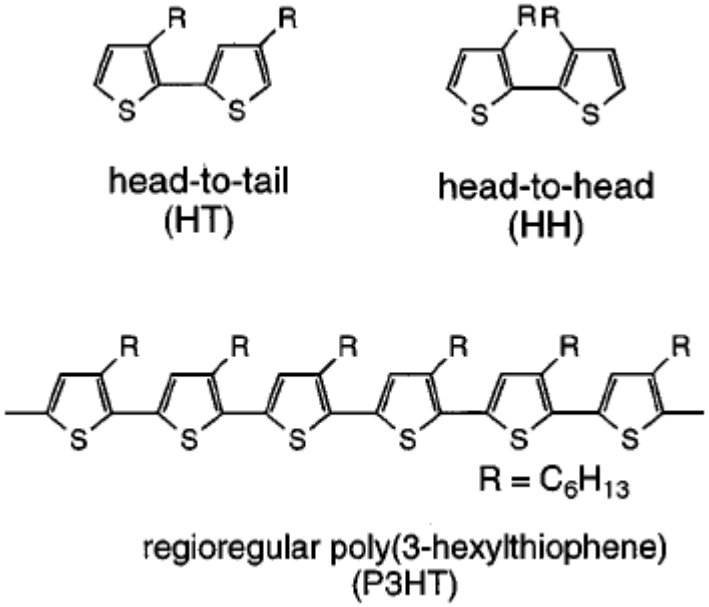

Fig. 1-4 The chemical structure of the P3HT [8]

According to the research of H. Sirringhaus *et al.*, in solution processes, the self-organization of conjugated polymers forms ordered microstructures, in which these micro-size domains are embedded in an amorphous matrix. In P3HT, the self-organization can result in lamellaes with two-dimensional conjugated sheets formed by interchain stacking as shown in Fig. 1-5 (a) [9]. The two-dimensional conjugated sheets may form a narowire-like structures (Fig. 1-5 (b)) when strong self-organization process occurs. As the P3HT was spin-coated on the substrate, the lamellae of P3HT have two orientations related to the substrate: normal and parallel to the substrate. Fig. 1-6 illustrates the two different orientations of P3HT. [10]

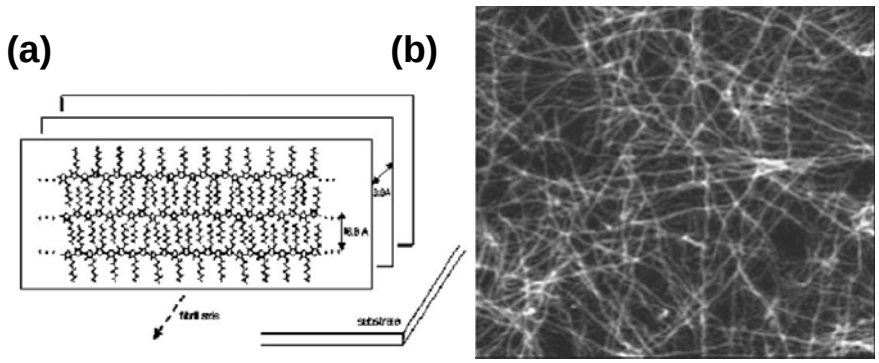

Fig. 1-5 (a) 2D conjugated P3HT lamellae (b) nanowire-like structures form by self-organization [9]

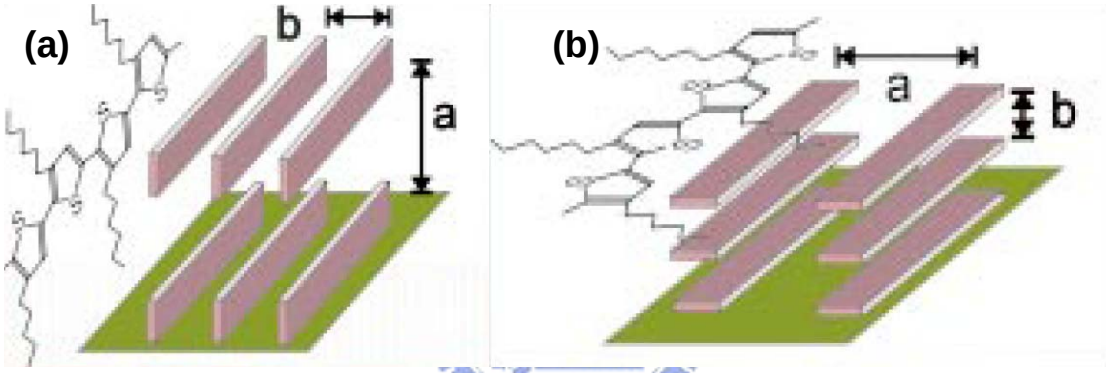

Fig. 1-6 Orientations of P3HT on the substrate (a) P3HT lamellae normal to substrate (b) P3HT lamellae parallel to substrate [10]

The regioregularity of P3HT is defined as the percentage of the head-to-tail structures in the P3HT. As high regioregularity (>91%) P3HT is spin-coated on the substrate, the preferential orientation is normal to the plane of substrate shown in Fig. 1-6 (a). In contrast, the preferential orientation of low regioregularity (81%) P3HT on the substrate is parallel to the plane of the substrate shown in Fig. 1-6 (b). [10] The current flow in P3HT-based TFT is along the plane of the substrate. The charge carrier transportation is limited by the π-π interchain rather than the intramolecular. The orientation of the π-π stacking determines the field-effect of the mobility. Fig. 1-7 shows that P3HT with higher regioregularity can result

in a higher field-effect mobility due to the parallel orientation of the π-π stacking between the self-organized conjugated sheets to the plane of the substrate. [10] The orientation of the lamellae of P3HT is possible normal to the plane of the substrate by dip casting. The dark triangle of 81% regioregularity denotes the as-cast films whose the mobility is higher than that of the spin coated films (the white triangle of 81% regioregularity) and slightly lower than that of the white triangle of 91% regioregularity. The possible reason is that the crystallites of low regioregularity P3HT have more time to arrange along the plane which is normal to the plane of the substrate in the case of the dip casting than in the case of the spin coating. [10]

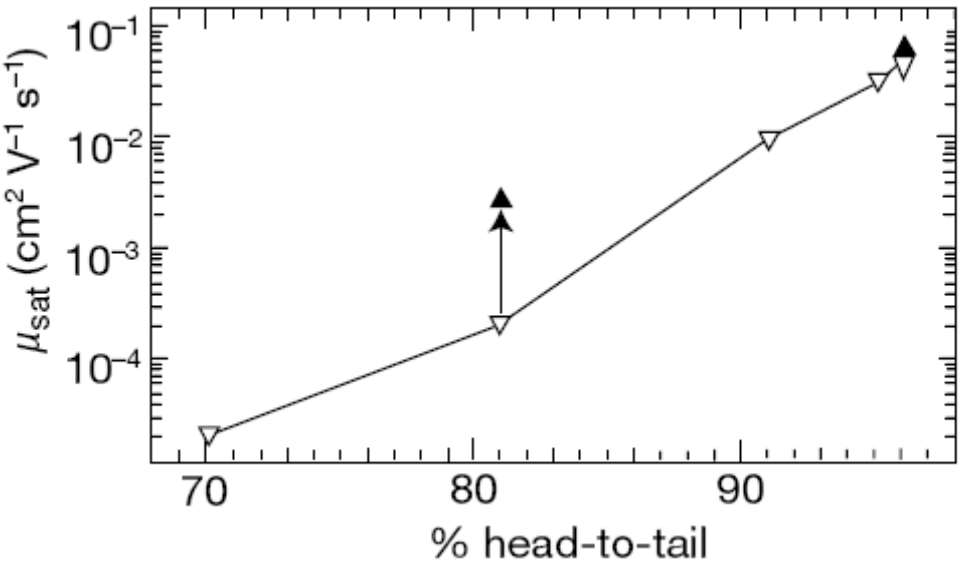

Fig. 1-7 The relation between field-effect mobility and regioregularity of P3HT [10]

The P3HT is a semiconducting material. Because of the overlaps of the electron orbitals, the energies of excitation states and the steady states of π electrons split into the highest occupied molecular orbital (HOMO) and the lowest unoccupied molecular orbital (LUMO). The HOMO and the LUMO are a concept that is similar to the energy band in inorganic semiconductors. The HOMO is analog to the valence band and the LUMO is

analog to the conduction band. The HOMO of P3HT is between -4.8 and -5.2 eV and the LUMO of P3HT is about from -2.7 to -3.0 eV according to different literature. The band gap of P3HT is about 2.0 eV as shown in Fig. 1-8. In order to increase the injection of carriers from a metal to P3HT, the metal work function must be close to the HOMO of P3HT to decrease the barrier at the interface. The work function of Au is -5.1 eV, which matches the HOMO of P3HT. Therefore, we selected Au as the source and drain metal in this study.

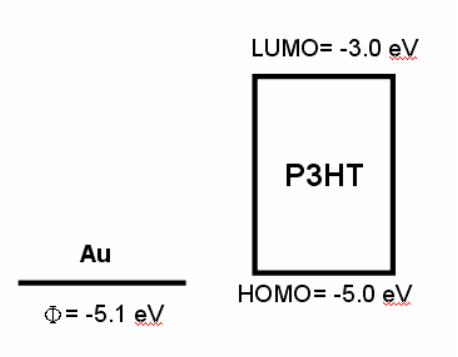

Fig. 1-8 Band diagram of Au and P3HT

1.4 Improvements of P3HT Thin-Film Transistors

Generally, the mobility of P3HT depends on the degree of head-to-tail regioregularity and the deposition conditions. [10-13] The dependence of the molecular weight of P3HT and the mobility has been addressed. [14,15] The length of the linear sidechain can affect the mobility of P3HT. [14,16,17] The mobility would decrease with increasing chain length. In addition, several solvents were tested to optimize the mobility of P3HT based transistors. [8,18,19]

The self-assembled monolayers (SAMs) were used to modify the silicon dioxide surface. The SAMs can transform the hydrophilic SiO_2 surface into hydrophobic surface. In addition, the SAMs with different functional groups were used to verify the ability of the arrangement for P3HT. [20,21] Different alkyl trichlorosilane was used to improve the performance of P3HT. [9,22,23] They concluded that the mobility depends on certain SAM

structure but not polarity or surface energy. [23]

The thermal annealing has been proved to improve the crystallization of P3HT. [14,24] On the other hand the solvent annealing has been applied to P3HT / PCBM system solar cell. [25,26] The solvent annealing is a new concept that is differ from the thermal annealing. The thermal annealing takes the heat energy to improve the arrangement of the active layer. However, the solvent annealing takes time to improve the ordering of the active layer by lowering the evaporation rate of the solvent of P3HT. By the assistance of the solvent, the self-organization of P3HT would help regularity of the active layer films. The solvent annealing on solar cell enhanced the short circuit current density and the power conversion efficiency. The same concept is also applied to P3HT transistors. [27-29] The strong self-organization effect of P3HT and the mobility enhancement were observed.

1.5 Structures of organic thin-film transistors

According to the position of source-drain electrode, organic thin-film transistors are divided into two structures: top contact and bottom-contact ones as shown in Fig. 1-9. The advantage of top contact structures is that there is a smaller contact resistance between the active layer and electrodes and the performance is better generally. But the channel length defined by the shadow mask can hardly decrease. The photolithography process is forbidden after the active layer deposition due to the fact that the removal of the photo resistance would damage the organic materials of the active layer. The TFTs with top contact structures has relative high off current because the back channel current flow near the source drain electrode. On the contrary, the TFTs with bottom contact structures have relative low off current. The channel length can be defined by photolithography. Because the active layer is deposited on the electrodes, the contact between the organic materials and the metals in the channel region is poor, hence resulting in high contact resistance and worse

performance.

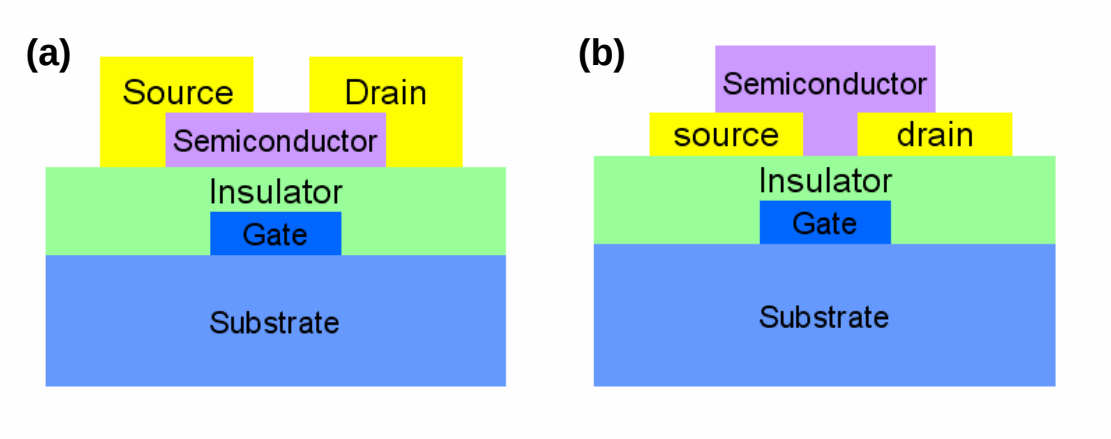

Fig. 1-9 Two TFT structures (a) Top contact (b) Bottom contact

1.6 Motivations

The thermal annealing and the solvent annealing can improve the mobility of P3HT. The thermal annealing makes the P3HT molecules vibrate by heating the P3HT films. Therefore, the molecules would approach to the thermodynamically stable state and the crystallinity increases after thermal annealing. On the other hand, the solvent annealing improves the mobility by extending the formation time of P3HT films. The solvent annealing seems to enhance the ordering of P3HT due to the self-organization of P3HT. In this article, the solvent annealing is applied to obtain uniformity P3HT films. Then, combining the solvent annealing and the thermal annealing, we expect to enhance the performance of P3HT transistors.

1.7 Thesis Organization

Chapter 1 introduces the background knowledge of materials and TFT structures

Chapter 2 explains the mechanism of the charge transportation in organic materials and the method of the parameter extraction in this article.

Chapter 3 describes the experiments and the measurement instruments used in this study.

Chapter 4 is divided into two parts. First, the results of the annealing effect on the P3HT-based TFTs are shown. Second, we analyze the device characteristics to understand the annealing effect.

Finally, chapter 5 gives the conclusions of our experiments.

Chapter 2

Mechanism and Operation

2.1 The Charge Carrier Transportation in Organic Semiconductors

The interaction between molecules in organic materials is van der Waals force. The van der Waals force is relative weaker than the covalent bonding between the atoms in inorganic materials. Hence the charge carrier transportation is quite different between organic and inorganic materials.

The π-bonding electron cloud has two states: localized states and delocalized states. The π-bonding electron is localized if the electron bound to particular atom. The localized π-bonding electron can not contribute to the carrier transportation. Fig. 2-1 shows the π-bonding electron states of benzene.

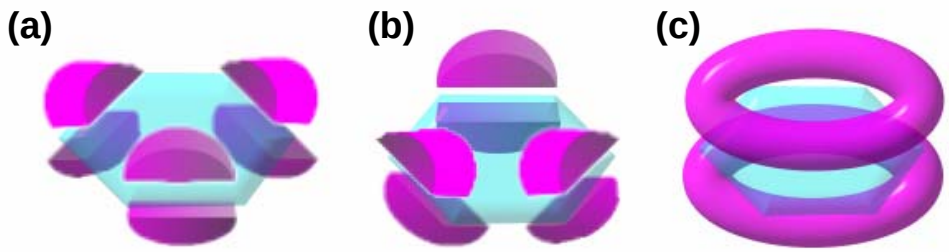

Fig. 2-1 π electron states (a),(b): localized states (c): delocalized states [30]

Generally, there are two models to describe the delocalized electrons transportation in organic materials, hopping model [31] and multiple trapping and release model (MTR) [32]

2.1.1 Hopping Model

In organic materials, the intermolecular transportation of charge carrier depends on hopping as shown in Fig. 2-2. This is the limitation of the charge carrier mobility in organic materials. Because the phonons would assist the hopping of carriers, the mobility increases with the increasing temperature. The relation between the mobility of the hopping and the temperature can be described as the following equation:

$$\mu = \mu_0 \exp[-(T_0 / T)^{1/\alpha}]$$

where the α is ranged from 1 to 4.

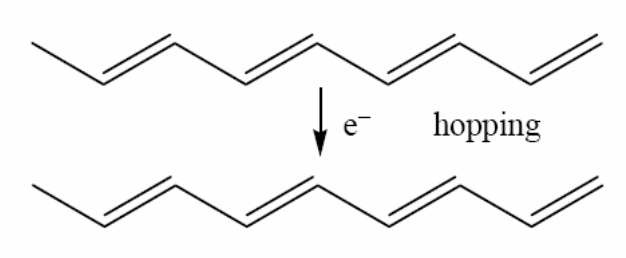

Fig. 2-2 Charge carrier hopping

2.1.2 Multiple Trapping and Release (MTR)

The MTR model is widely used in a-Si semiconductors. In MTR model, it assumes that there exist localized levels in the band gap due to defects. These localized levels are like traps for charge carriers. These levels would form a narrow band with high concentration of trap levels. When the charge carriers transport to the levels, the carriers would be trapped with the probability near 100%. On the other hand, the activation energy of the carrier determines the release of the carrier. The released carrier would contribute to the transportation and the drift mobility is given as following:

$$\mu_D = \mu_0 \alpha \exp(-E_t / kT)$$

where E_t is the energy level of the defects, α is the ratio between the density of states at the bottom of the band and the density of traps.

2.2 The Operation of Organic TFT

In n-type silicon MOSFETs, the source drain terminates are highly n-doped and the bulk semiconductor is p-doped. The transistor is in OFF state. When a positive voltage biased at the gate, the hole near the semiconductor / insulator interface are repelled and the electrons start to accumulate thus form a channel between source and drain. This transistor is operated in inversion mode.

The organic thin-film transistors are operated in accumulation mode. When the gate biases a negative voltage, the holes would accumulate in the interface between the active layer and the insulator. If there are enough holes to accumulate in the interface, the channel is formed and the transistor is in ON state. When the drain is biased at a negative voltage, the drain current would flow from the source to the drain. Fig. 2-3 illustrates the operation of the p-type organic transistor.

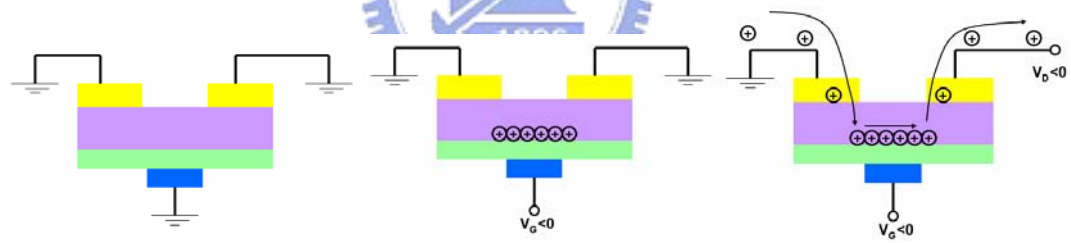

Fig. 2-3 Operation of OTFT

The transistor is a three-terminal device. There are two transfer characteristics plots. The first plot is I_D-V_D characteristics as shown in Fig. 2-4. The I_D versus V_D relation is measured under several constant V_G. The transfer characteristics are separate into two regimes. The linear regime occurs when V_D approaches to zero. The transistor behaves as a resistance. When V_D is increasing, the transistor would be in the saturation regime. In saturation regime, the I_D is governed by V_G.. The second plot is I_D-V_G transfer characteristics as shown in Fig. 2-5. From the I_D-V_G plot, many parameters like the mobility

and threshold voltage can be extracted.

2.3 The Parameters Extraction of Organic Thin Film Transistors

Although the transportation mechanism in organic materials is different from that of inorganic materials, the transfer characteristics are similar. The formula derived from the inorganic semiconductors was adopted to calculate the parameters like the field-effect mobility and threshold voltage in this article.

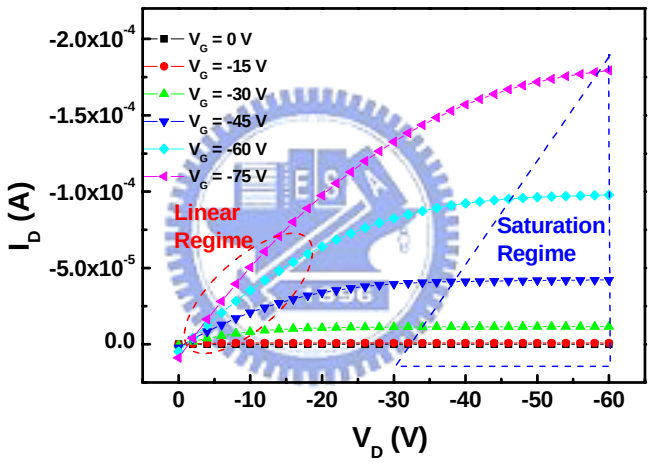

Fig. 2-4 I_D-V_D output characteristics plot of the p-type transistor

The typical p-type I_D-V_D transfer characteristics is shown Fig. 2-4. When the TFT is operated at linear regime, the drain current is governed by the equation 2-1.

$$I_D = \frac{WC_i}{L}\mu(V_G - V_T - \frac{V_D}{2})V_D \qquad (2\text{-}1)$$

where W is the channel width in cm, L is the channel length in cm, C_i is the capacitance per unit area in F/cm^2, μ is the field-effect mobility in cm^2/Vs, the Vt is the threshold voltage in Volt.

When $V_D > V_G - V_T$, the TFT is operated at saturation regime. The drain current is given by the equation 2-2.

$$I_D = \frac{WCi}{2L}\mu(V_G - V_T)^2 \qquad (2\text{-}2)$$

The μ can be calculated by differentiating the square root of I_D in saturation regime

$$\left(\frac{\partial\sqrt{|I_D|}}{\partial V_G}\right)_{V_D=const} = \sqrt{\frac{WC_i}{2L}\mu} \qquad (2\text{-}3)$$

The slope can be obtained from the I_D-V_G transfer characteristics plot shown in Fig. 2-5. The fitting line of the square root of I_D in $I_D^{1/2}$-V_G plot in the saturation regime, the intersect of the line and the x-axis is the V_T. The turn on voltage V_{on} and the on/off ratio can be obtained form the I_D-V_G transfer characteristics plot.

The subthreshold swing is a parameter to determine the switch speed of a transistor. It can be calculated by equation 2-4.

$$S.Swing = Min\left[\left(\frac{\partial\log(|I_D|)}{\partial V_G}\right)^{-1}{}_{V_D=const}\right] \qquad (2\text{-}4)$$

The dimension of subthreshold swing is V/decade. The subthreshold swing gives the degree of the switch property of a transistor.

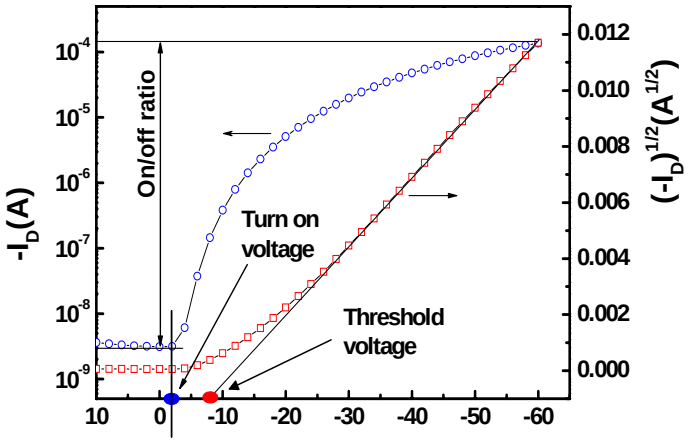

Fig. 2-5 I_D-V_G transfer characteristics plot of the p-type transistor

Chapter 3

Experiments

3.1 The Materials

The head-to-tail regioregular poly(3-hexylthiophene) (or as called HT rr-P3HT) that is shown in Fig. 3-1(a) was used in the active layer of thin-film field-effect transistors. We dissolved the P3HT in the 1,2-dichlorobenzene (o-DCB) or in the chloroform. In order to improve the performance, the gate/active layer interface was modified with the self-assembled monolayers (SAMs). Here we used three materials to be our SAMs, which are octadecyltrichlorosilane (OTS), octadecyltrimethoxysilane (OTmoS), and 3-[2-(2-Aminoethylamino)ethylamino]propyltrimethoxysilane (APTMS or NH2 terminated). The SAMs was dissolved in the toluene, hexane, or heptane. The chemical structures of materials mentioned are shown in Fig. 3-1.

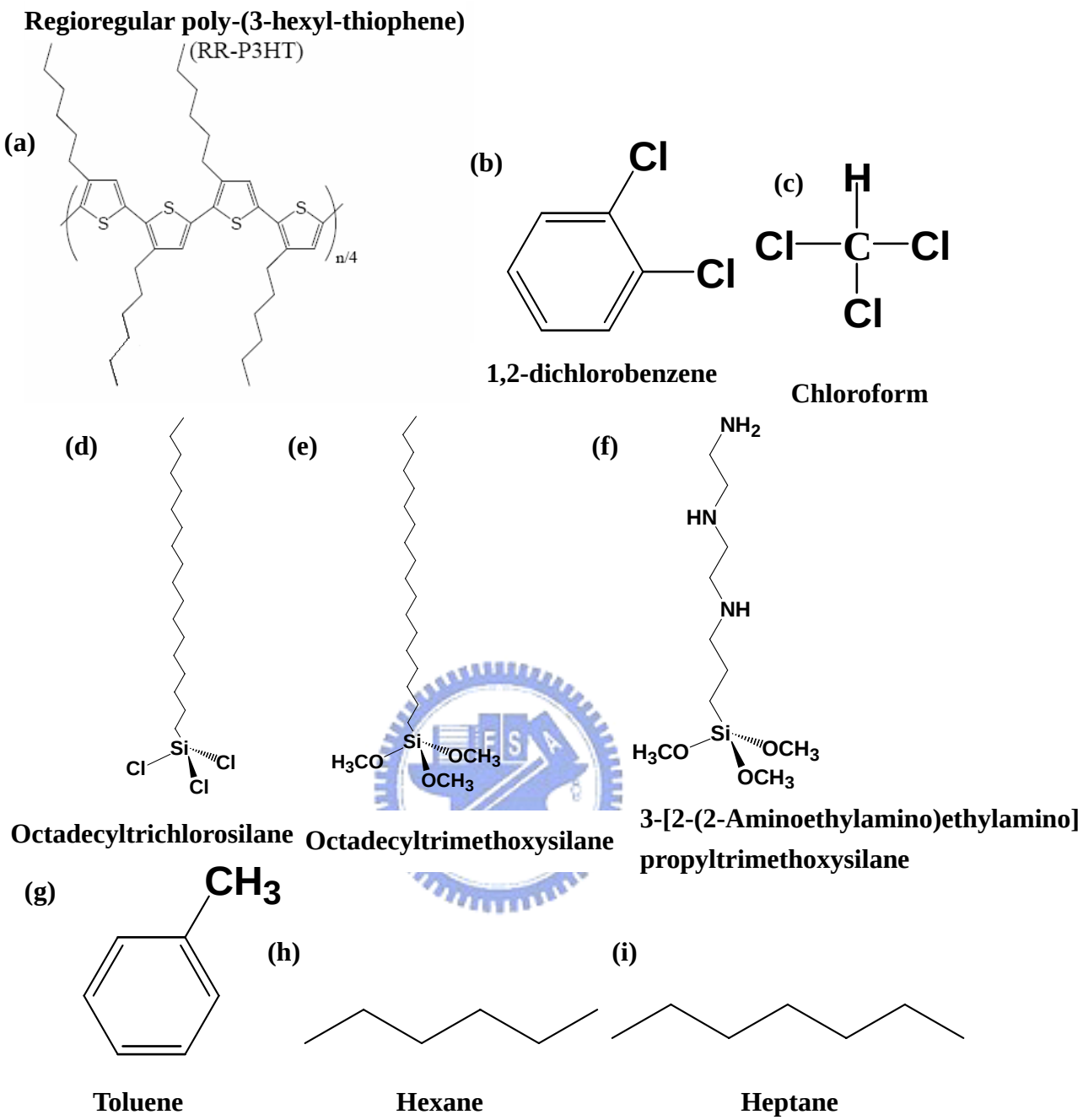

Fig. 3-1 The structure of materials that used in experiments.

3.2 The Device Fabrication

3.2.1 Substrates Preparation

The substrates were highly As doped silicon wafers. Their resistance was about 0.001~0.003 ohm-cm. The conductance of the wafers is high enough to serve as the gate electrode. By using thermal growth, we deposit about 200 nm SiO_2 on the wafers as the gate insulator. The measured capacitance per unit area is about 14.1 nF/cm^2.

We rinse our substrates with DI (de-ionized) water for 5 minute to remove large particles. Then the substrates are rinsed with the mixture of H_2SO_4 and H_2O_2 for 10~15 minute. The mixed ratio is H_2SO_4:H_2O_2=3:1. H_2SO_4 and H_2O_2 are strong oxidant and capable of removing chemical substances. In order to remove the residual mixture H_2SO_4 and H_2O_2, the wafers are rinsed with DI water for 5 minute. Finally, we use the nitrogen gun to blow our wafers to remove the residual water. After the first steps of RCA cleaning, the wafers are placed into an oven which the temperature is set to 120℃ for over night to remove the crystal water.

3.2.2 The Device Fabrication

As the wafers were prepared, the devices were fabricated by following steps:

1. The surface treatment of the gate/active layer interface.
2. To spin coat the P3HT as the active layer.
3. To treat the devices with the solvent annealing.
4. To treat the devices with the thermal annealing.
5. To evaporate gold onto the devices as the electrode.

The detail of each step is discussed as followings.

The surface treatment of the gate/active layer interface

Before the deposition of the active layer, we often treat the surface of the wafers with the organic material. Generally speaking, there exist many defects in the interface between the inorganic material and the organic material because the different surface properties. In the operation of the OTFT, the current flow in the channel is near the interface and the transportation of charge carriers is affected dramatically by the defects. Furthermore, the crystalline orientation of regioregular P3HT and its conformational stability can be improved by the functionalized SAMs. With increasing molecular ordering of P3HT, the characteristics of OTFT devices will get better. [20]

In our experiment, three different SAMs: APTMS (NH2 terminated), OTS, and OTmoS were used to modify the gate/active layer interface. Due to their different activities, the concentration of the solutions and the immersing time of SAMs were changed.

In the case of the SAMs of APTMS, APTMS was dissolved in the toluene and the concentration is 1mM. The prepared substrates were immersed in the solvent for 20 seconds to obtain the monolayers. Then the substrate were rinsed by the toluene to remove residual reactant and were dried by nitrogen.

In the case of the SAMs of OTS, the concentration was 1mM but the solvent used was hexane. The immersing time was about 1 minute.

In the case of the SAMs of OTmoS, the concentration was 75mM and the OTmoS was dissolved in the hexane as the same as OTS. Before immersing OTmoS, the substrates were treated with UV-ozone for 15 minute to increase –OH groups on the wafers. The immersing time was 30 minute.

Spin coating of the P3HT as the active layer

The rr-P3HT was obtained from the Rieke Metals, Inc. The films of active layer of P3HT were spin coated from a 0.6 wt% solution in 1,2-dichlorobenzene (o-DCB) on the

surface-treated substrate in the glove box which filled with nitrogen. The spin rate was set to 600 rpm for 60 seconds to obtain uniform films.

To treat the devices with the solvent annealing

Because the low spin rate, there was still a large amount of solution left on the device after spin coating. We controlled the evaporation rate of the residual solution to be slower than the usual case. By placing the device into a smaller container, the evaporation rate decreased because only little amount of solvent evaporated to the small container and the saturation vapor pressure were reached easily. All devices were placed in small Petri dishes until the residual solution dried.

Thermal annealing

For most organic electronic devices, the annealing temperature is an important factor. The performance of organic electronic devices can be improved via heating devices with a proper temperature. After solvent annealing, the residual solution on devices had dried. And we placed devices on a 110℃ pre-heated hotplate for 15 minutes. Then all devices were placed in a room temperature environment to cool down.

Evaporation gold onto the devices as the electrode

We used gold (Au) as our TFT electrode material. Gold was evaporated by a thermal coater with about 3 Å/s evaporation rate. While gold evaporation, the pressure of the chamber keep under 3×10^{-6} torr to avoid impurities to evaporate onto devices. The pattern of source drain electrode was defined by the shadow mask. The designed channel width was 2 mm and channel length was in the range from 75 μm to 160 μm. The ratio of channel width over channel length ($\frac{W}{L}$) was about from 12 to 30.

Fig. 3-2 illustrates the standard processes of the experiments.

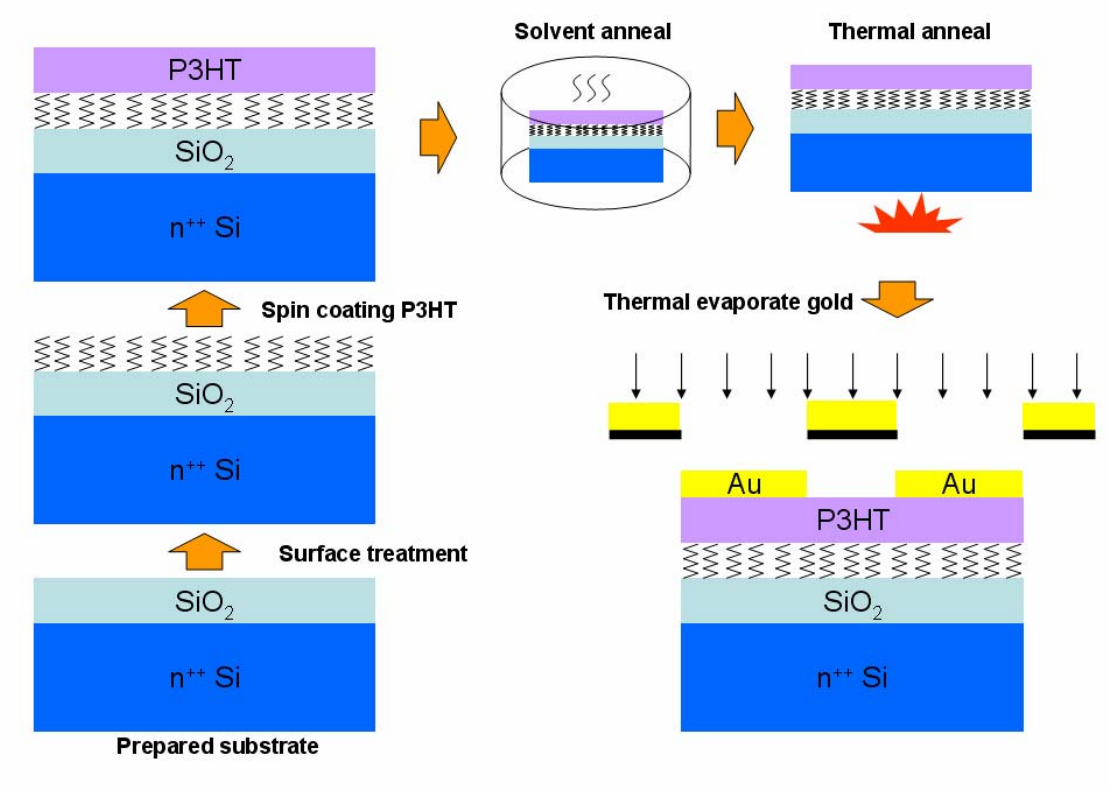

Fig. 3-2 Demonstration of the experiments flow

3.3 The Device Measurement

3.3.1 I-V Characteristics Measurement

The measurement instrument in our experiments is Keithley 4200 Semiconductor Characterization System. Hence we applied a negative voltage at the gate to accumulate holes and form a channel in the semiconducting active layer near the insulator / active layer interface. At the same time, we applied another negative voltage at drain to pull holes from the source. In the Id-Vd characteristics measurement, we selected 0, -15, -30, -45, -60 Volt to apply the gate voltage and swept the drain voltage from 0 to -60 Volt. In the Id-Vg characteristics measurement, we biased 0, -15, -30, -45, -60 Volt on the drain terminal and swept the gate voltage from 40 to -60 Volt. While measuring, the TFT devices were enclosed by an electromagnetic waves-shielded box to avoid the interference from the

environment.

3.3.2 Surface Morphology Measurement

We used the tapping-mode atomic force microscope (AFM) to obtain the surface morphology of the active layer. By the interaction of the van der Waals force between the tip of the cantilever and the surface topology of the sample, the cantilever vibrates due to the magnitude of the interaction. Detecting a laser beam reflected by the cantilever can sense the tiny vibration of the cantilever. The computer record these detected signals and construct the surface morphology of samples. Fig. 3-3 illustrates the structure of AFM. From the surface morphology, we have clues to realize the relation between the device performance and the morphology of the active layer.

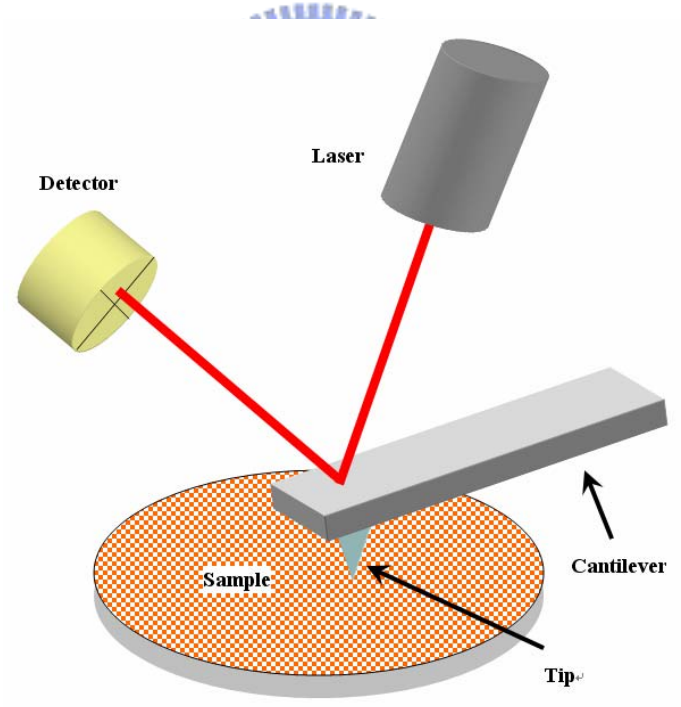

Fig. 3-3 A schematic of an atomic force microscope

While a tapping-mode AFM measuring, the probe oscillates up and down regularly. It prevents the probe to damage the surface of the samples and obtains extra information about

the samples. The computer records the feedback amplitude and the phase signals of the cantilever. From the amplitude signals we can obtain the morphology information. The phase signals reveal the different materials or structures of the sample.

Chapter 4

Results and Discussions

4.1 The Effect of the Annealing

4.1.1 The Effect of the Thermal Annealing

Fig. 4-1 shows the effect of thermal annealing at 110℃ for 15min. The two devices were also treated with solvent annealing. The average mobility increased by the factor of 1.3 from 1.3×10^{-3} cm^2/V-s to 1.7×10^{-3} cm^2/V-s.

From Fig. 4-2, both the electrical characteristics were very similar. The V_{on} of the device without thermal annealing showed in Fig. 4-2 (a) is 12 V and the one with thermal annealing showed in Fig. 4-2 (b) is 16 V. The subthreshold swings were 4.6 V/decade and 4.0 V/decade respectively. From the results, the thermal annealing effect can improve the characteristics of the devices.

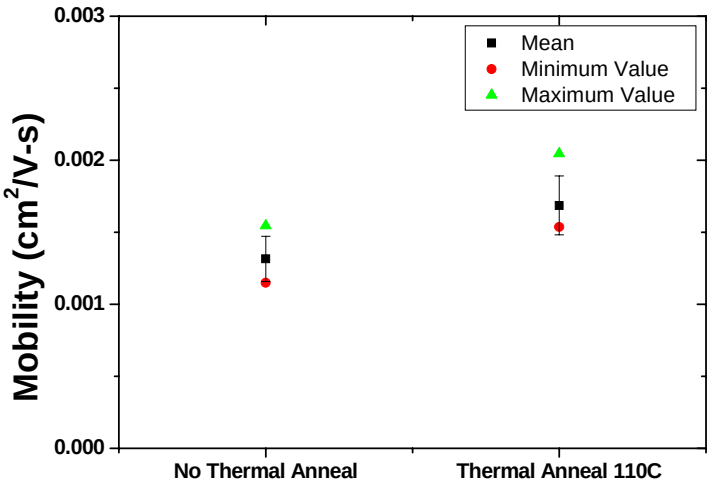

Fig. 4-1 The mobility enhancement of with thermal annealing treatment

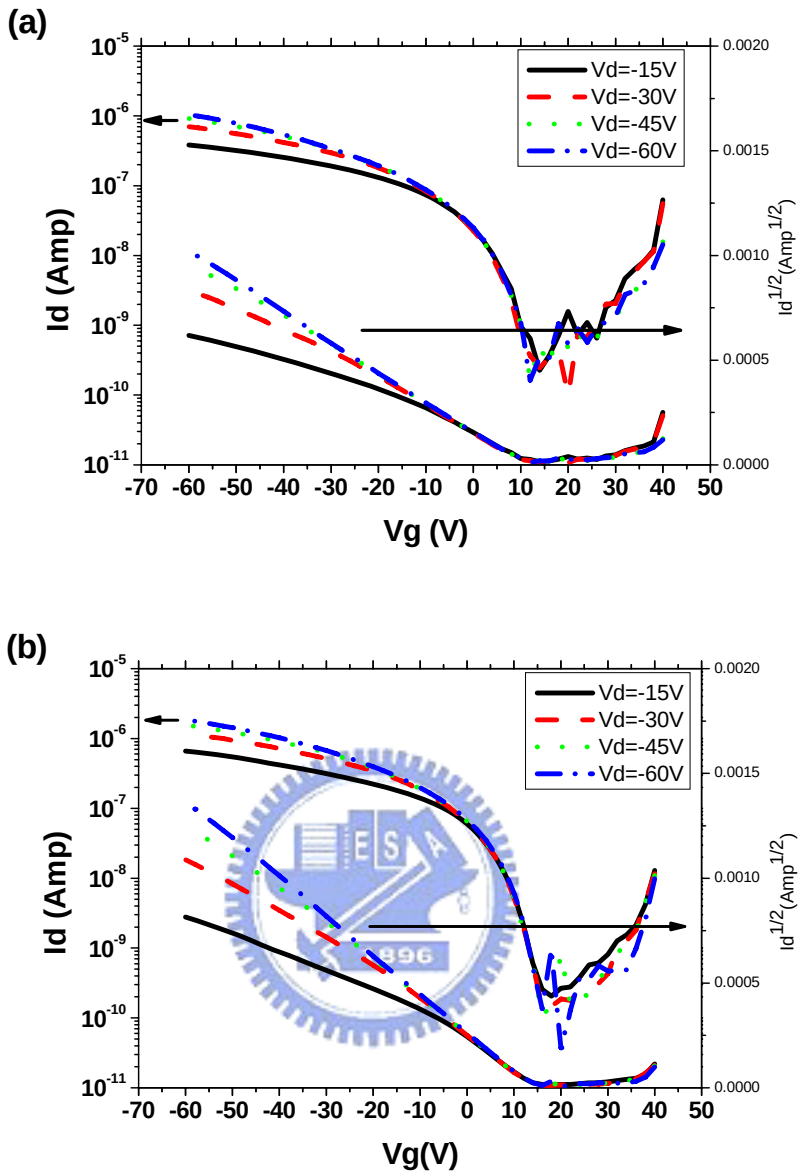

Fig. 4-2 Id-Vg characteristics (a) without thermal annealing treatment (b) with thermal annealing treatment

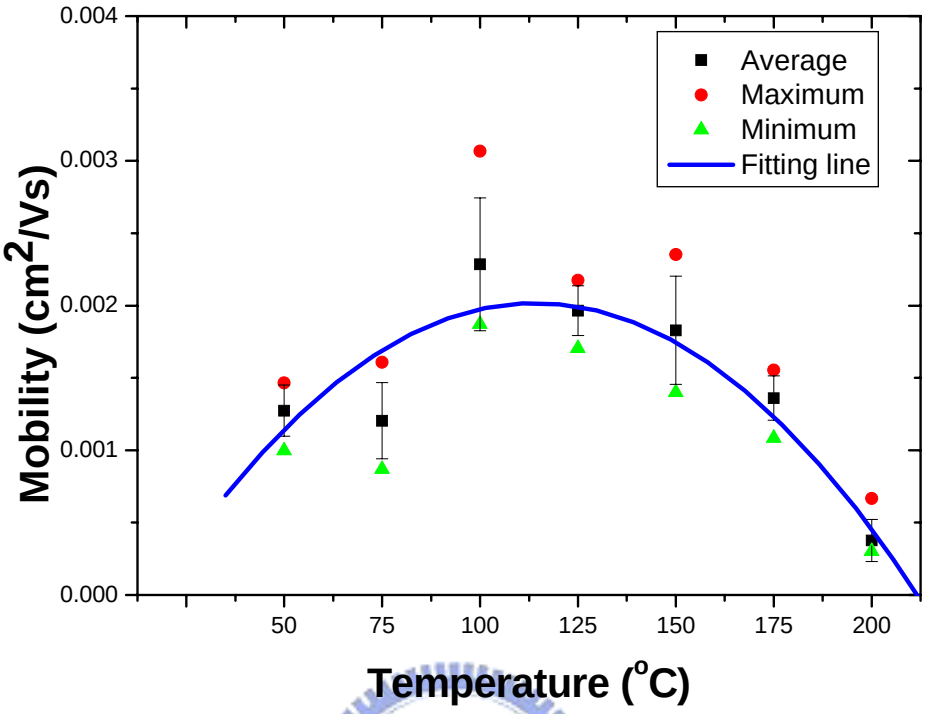

Fig. 4-3 The mobility vs. different temperature thermal annealing

In order to optimize the temperature of thermal annealing, several temperatures were tested. Fig. 4-3 shows the relationship between mobility and annealing temperature. The figure points out that the devices have the highest mobility between 100 ℃ and 125 ℃. Thus we choose 110 ℃ as the optimized annealing temperature in our experiments. As the annealing temperature was above 125 ℃, the mobility decreased with increasing temperature.

4.1.2 The Effect of the Solvent Annealing

A P3HT-based TFT device, the orientation of the conjugated sheets formed by self-organized P3HT affects the FET mobility significantly. (see Chapter 1.3 for detail) In a solvent annealing process, the main purpose was to decrease the evaporation rate of P3HT solution. In practice, we placed the devices with solution in a small Petri dish. The evaporation rate of P3HT solution decreases due to the saturated vapor pressure. If the evaporation rate is slower, P3HT have more time to form the orientation that normal to the substrate.

The device A was treated without any annealing process. The device B was annealed at 110 ℃ for 15 minutes. The device C was treated with solvent annealing only. The device D was treated with both the solvent annealing and the thermal annealing (at 110 ℃ for 15 minutes).

Fig. 4-4 shows the mobility enhancement with annealing treatment. Comparing the devices of B and D in Fig. 4-4, the two devices were both annealed at 110℃ for 15 minutes. The solvent annealing treatment would increase the mobility of the devices by 2.4 times, from 0.7×10^{-3} to 1.7×10^{-3} cm2/V-s.

The solvent annealing is more efficient in increasing the mobility than the thermal annealing. The mobilities of solvent annealed devices were increased from 4×10^{-4} to 1.3×10^{-3} cm2/V-s. But the mobilities of thermal annealed devices were only increased from 4×10^{-4} to 7×10^{-4} cm^2/V-s. The mobility can be improved further by combining both the solvent annealing and the thermal annealing. Finally, the mobility can be raised from 4×10^{-4} to 1.7×10^{-3} cm^2/V-s without gate insulator modification.

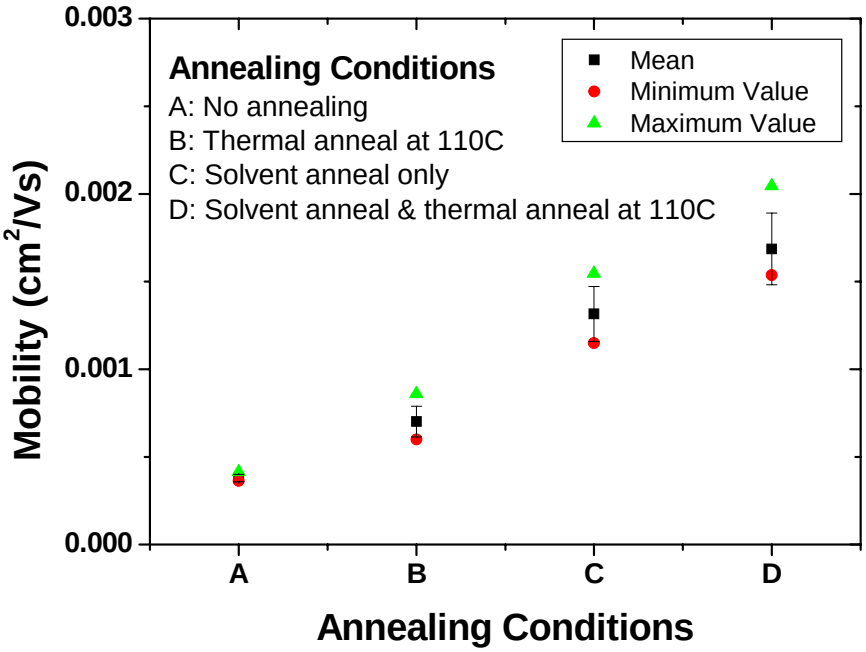

Fig. 4-4 The mobility enhancement with annealing treatment

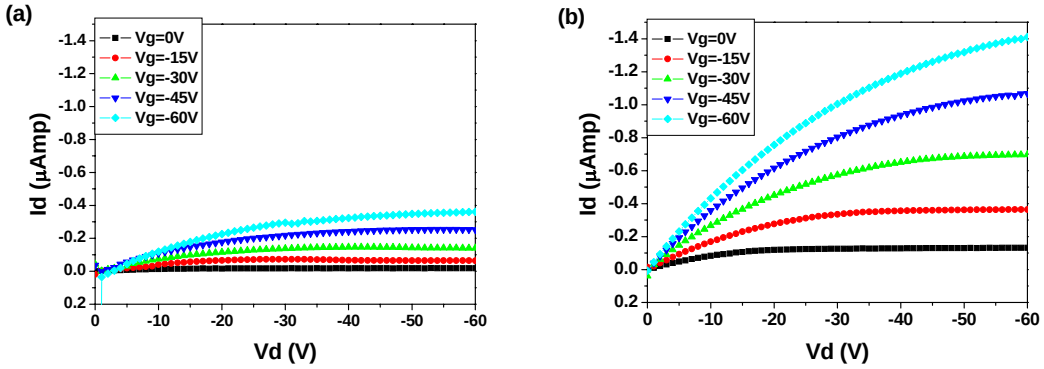

Fig. 4-5 I_d-V_d characteristics (a) no solvent annealing treatment (b) with solvent annealing treatment

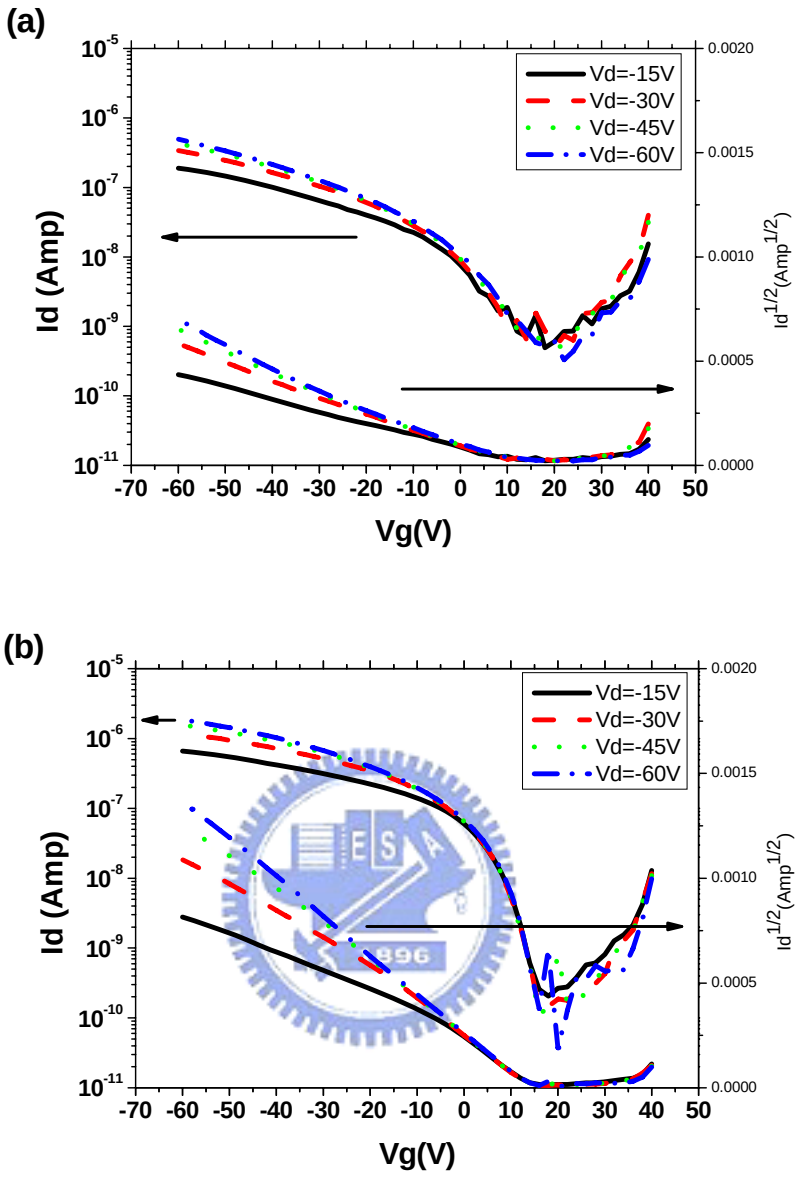

Fig. 4-6 I_d-V_g characteristics (a) without solvent annealing treatment (b) with solvent annealing treatment

Fig. 4-5 and Fig. 4-6 show the characteristics of the device. In the Id-Vd transfer characteristics, the magnitude of the saturated I_d current increased from 0.36 μA to 1.4 μA with -60 V biased at the gate voltage. In the I_d-V_g transfer characteristics, the mobility that we extracted from Fig. 4-6 (a) was 7×10^{-4} cm^2/V-s and the mobility that we extracted form Fig. 4-6 (b) was 2×10^{-3} cm^2/V-s. The on / off ratio also increased from 3 orders to 4

orders due to the increasing field-effect mobility. The V_t were -0.4 V and 12.8 V but the V_{on} were 18 V and 16 V respectively. Here we observed that the solvent annealing treatment does not change the position of the turn on voltage. With solvent annealing treatment, the subthreshold swing decreased from 11.1 V/decade to 4.0 V/decade. It means that we need less voltage to operate the switching of the TFT devices.

4.1.3 The Solvent Annealing Effect on Other Processes

The solvent annealing is not an independent process. Many processes may involve the solvent annealing effect like the spin rate or the choice of the different boiling point solvent of P3HT.

The spin rate effect

In solution processes, an important parameter is the spin coating rate and the polymer concentration in solvent. Different spin rate and P3HT concentration versus the mobility is shown in Fig. 4-7. For the three different concentration of P3HT, the concentration of 0.6 wt% has higher mobility. The lower spin coating rate resulted higher mobility for any P3HT concentration. Table 4-1 summarizes that the concentrations of 1.5 wt% and 2.5 wt% had slightly lower mobilities than the concentration of 0.6 wt%, but the on / off ratio decreased from 4 orders to 2 or 1 order. Because of the high concentration of the P3HT solution, the P3HT films hardly to turn off and resulted in high off current. The high off current seemed to have no apparent relations with the thickness from Table 4-1. We conclude the 0.6 wt% of the three concentrations was suitable to be in the P3HT-based thin-film transistors.

Comparing of the thickness versus the mobility, the mobility of the same film thickness (e.g. the 600 rpm, 0.6 wt% and the 2000 rpm, 1.5 wt% devices) is much different. The difference of mobility of 0.6 wt% devices is much large than the difference of the film thickness. It implies that the relation between mobility and the film thickness does not exist.

Consequently, the mobility of P3HT-based transistors doesn't depend on the film thickness but on the properties of the P3HT films.

From Fig. 4-7, there is a significant drop of the mobility between the spin rate of 1000 rpm and 2000 rpm. However, the film thickness showed in Fig. 4-8 doesn't have such drop. Depending on the observation during the experiments, the solvent annealing effect played an important role in the process. When the spin rate above 2000 rpm, the P3HT solution had almost dry due to the high speed circular motion. Hence the solvent annealing effect did not exist in the spin rates that were higher than 2000 rpm. In contrary, if the spin rates were lower than 1000 rpm, the P3HT solution remained on the substrates. The higher were the spin rates, the less solution would remain on the substrates and the solvent annealing effect would be more profound. The phenomenon resulted in that the devices with the spin rate of 600 rpm had the highest mobility and best transfer characteristics.

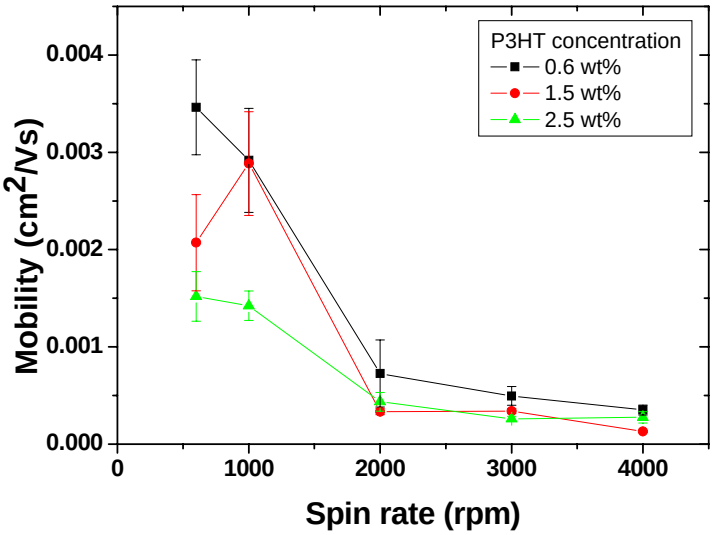

Fig. 4-7 The mobility versus the spin rate of the spin coating

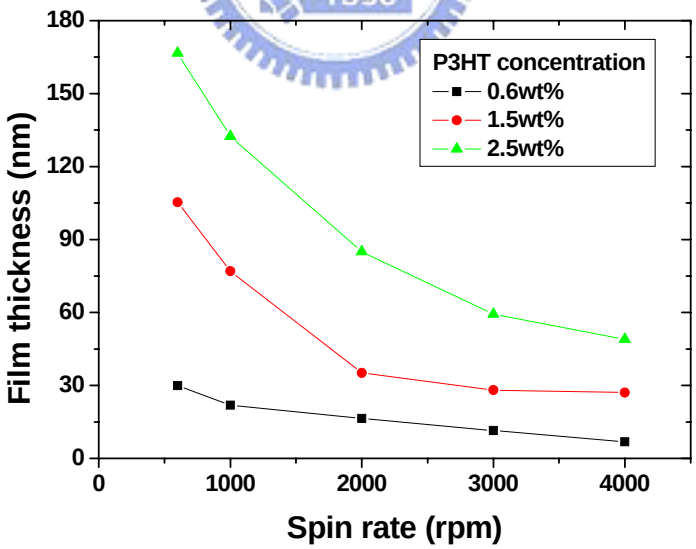

Fig. 4-8 The film thickness at different spin rate and P3HT concentration

Table 4-1 The parameters of different concentrations and spin rates

P3HT concentration (wt%)	Spin rate (rpm)	Mobility (cm^2/Vs)	V_t (V)	V_{on} (V)	On/Off ratio	Off current (Amp)	S.Swing (V/decade)
0.6	600	0.0040	2.3	4	2×10^{4}	1×10^{-10}	2.14
	1000	0.0034	1.6	6	1×10^{4}	2×10^{-10}	3.67
	2000	0.0008	-2.6	8	2×10^{3}	4×10^{-10}	8.78
	3000	0.0006	6.1	4	7×10^{2}	5×10^{-10}	6.49
	4000	0.0003	-3.5	6	4×10^{2}	3×10^{-10}	11.6
1.5	600	0.0030	26.2	32	3×10^{2}	6×10^{-9}	13.82
	1000	0.0035	25.8	32	4×10^{2}	5×10^{-9}	10.94
	2000	0.0003	10.4	14	4×10^{2}	6×10^{-10}	8.74
	3000	0.0003	2.5	10	4×10^{2}	6×10^{-10}	8.04
	4000	0.0001	21.3	18	1×10^{2}	2×10^{-9}	13.44
2.5	600	0.0020	53.9	38	2×10^{1}	1×10^{-7}	23.08
	1000	0.0016	23.8	26	4×10^{2}	2×10^{-9}	9.93
	2000	0.0005	34.0	32	4×10^{1}	3×10^{-9}	20.66
	3000	0.0003	34.2	30	7×10^{1}	3×10^{-9}	16.83
	4000	0.0002	38.7	24	3×10^{1}	6×10^{-9}	19.73

The solvent effect

The different solvent of P3HT could affect the transfer characteristics of transistors. We tested the 1,2-dichlorobenzene (o-DCB) and the chloroform to examine the relation

between the solvent annealing effect and the boiling point of the solvent. The boiling point of o-DCB is about 180 ℃ and the boiling point of chloroform is about 61 ℃. The solvent with low boiling point has faster evaporation rate and has small solvent annealing effect. Fig. 4-9 shows the I_d-V_d transfer characteristics of the P3HT solved in o-DCB and chloroform respectively, and spin coated on OTS treated substrates. As expected, the P3HT solved in o-DCB had higher current than the P3HT solved in chloroform due to the solvent annealing effect. For chloroform based devices, the solvent had dried after spin coating but the solvent of o-DCB had remained on substrates.

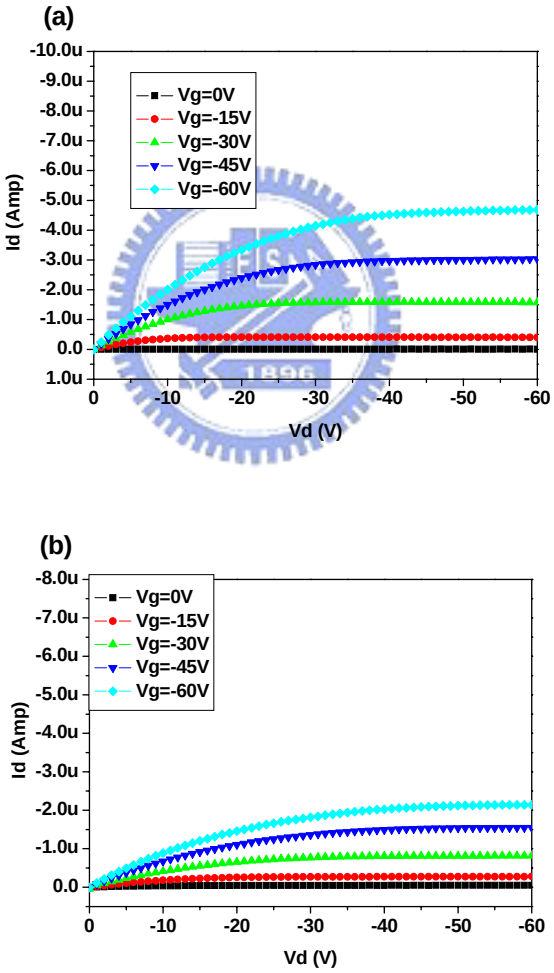

Fig. 4-9 Id-Vd characteristics of different P3HT solution (a) o-DCB (b) Chloroform

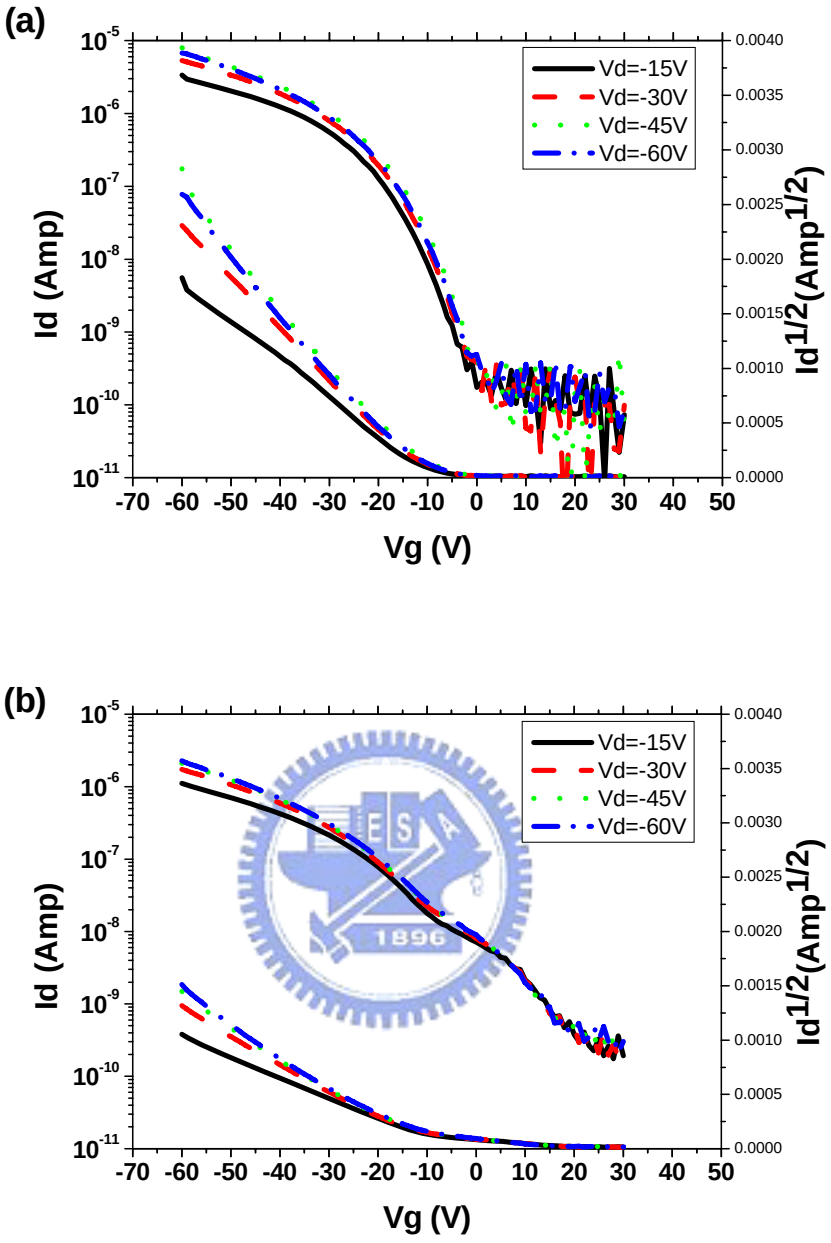

Fig. 4-10 Id-Vg characteristics of different P3HT solution (a) o-DCB (b) Chloroform

Table 4-2 Parameters of the different solvent of P3HT

	Mobility (cm^2/Vs)	V_t (V)	V_{on} (V)	On/Off ratio	S.Swing (V/decade)
o-DCB	0.0213	-12.8	2	3×10^4	4.72
Chloroform	0.0070	-11.5	14	1×10^4	12.03

The I_d-V_g plot is shown in Fig. 4-10. The devices with P3HT solved in o-DCB have higher field-effect mobility and better subthreshold swing. The devices with chloroform had poor transfer characteristics about the subthreshold swing. Table 4-2 summarizes the parameters of the two different solvent of P3HT. The mobility and the subthreshold swing had 3 times enhancement. In summary, the devices with P3HT solved in chloroform have poor performance due to its low boiling point (61 ℃). The low boiling point would cause the high solvent evaporation rate and less formation time of P3HT films. Hence, the solvent annealing might affect the devices with P3HT solved in o-DCB and results in better conformations of P3HT films.

4.2 The Analysis of the Annealing Effect

4.2.1 The Morphologic Analyses of the Solvent Annealing

In order to study the morphology of P3HT films and the annealing effect, the different of annealing condition were measured by the atomic force microscope. Four different annealing conditions were prepared: neither thermal annealing nor solvent annealing devices, thermal annealing devices, solvent annealing devices, and both solvent and thermal annealing, respectively. Fig. 4-11 shows the morphologies of the different conditions. The difference in height become more obvious whatever after thermal annealing or solvent annealing. The roughness also increased after either annealing. From the summary in Table 4-1, we find that there is a positive relationship between the roughness and the mobility. But there are not sufficient clues to determine the cause. A reasonable guess is that the mechanism of self-organization of P3HT results rougher surface. [26] Since we know that the self-organization affects the film quality significantly, the mobility increased with the more order P3HT films. Both thermal annealing and solvent annealing can improve the self-organization of P3HT and result in high mobility. Finally, the self-organized P3HT films would have rougher surface morphology.

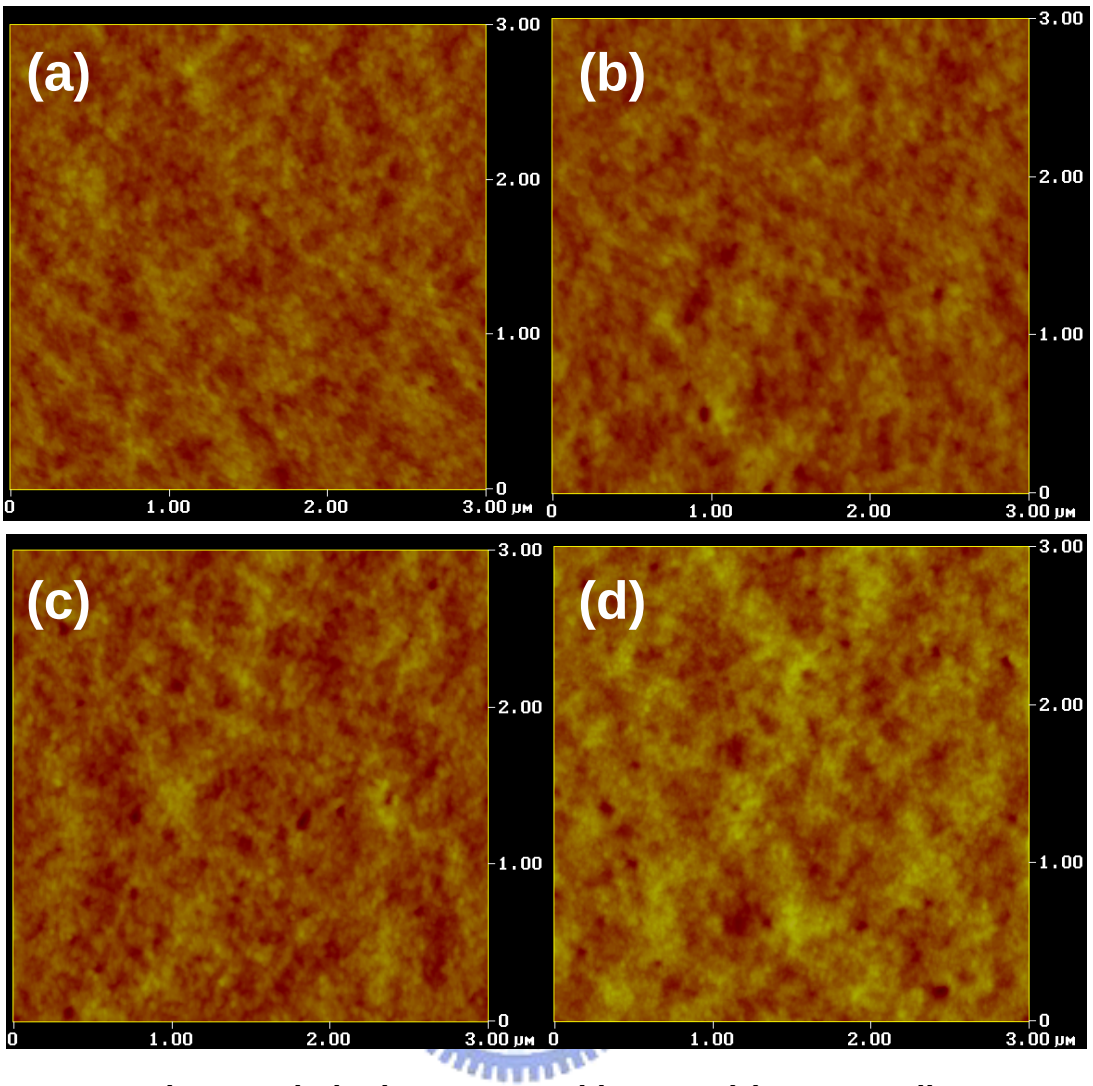

Fig. 4-11 The morphologies measured by AFM (a) no annealing treatment. (b) thermal annealing treatment. (c) solvent annealing treatment. (d) solvent annealing and thermal annealing treatment.

Table 4-3 Summary of morphology

	No annealing	Thermal annealing	Solvent annealing	Solvent annealing & thermal annealing
Roughness (nm)	2.508	2.573	2.931	3.302
Z range (nm)	23.028	23.776	31.551	36.187
Film thickness (nm)	37.00	37.97	37.28	45.35
Mobility (cm^2/Vs)	0.0004	0.0009	0.0012	0.0019

Fig. 4-12 shows the morphology of the different spin coating rate with 0.6 wt% P3HT solution. The complexity of surface morphology becomes simpler with the increasing spin rate. From the summary in Table 4-4, there still exist a positive relationship between the mobility and the roughness. We see that the morphologies caused by the self-organization of P3HT reduced with the increasing spin rate. It interprets that the lower mobility devices with high spin rate. As mentioned in chapter 4.1.3. , there is a significant drop of mobility between the 1000 rpm and the 2000 rpm due to the solvent annealing effect. The self-organized P3HT would form nanowire-like structures. Note Fig. 4-12 (b) and (c), the dramatic reduction the nanowire-like structures are probably the cause of the decreasing mobility.

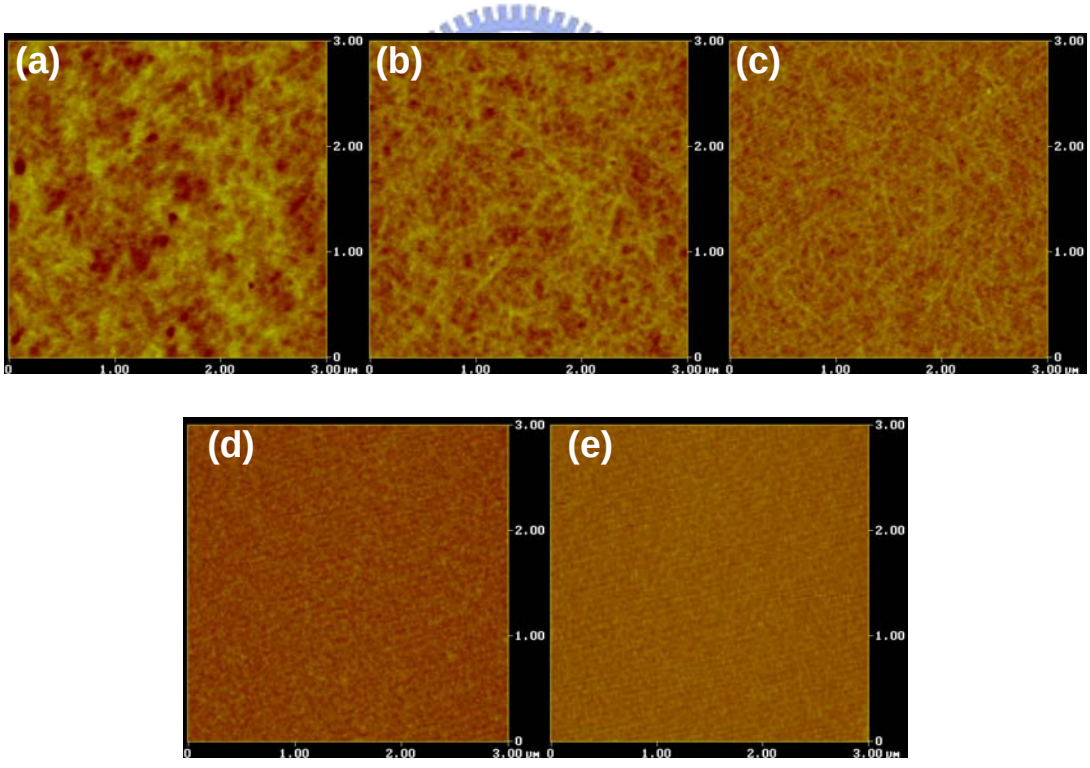

Fig. 4-12 The morphology of different spin coating rates: (a) 600 rpm (b) 1000 rpm (c) 2000 rpm (d) 3000 rpm (e) 4000 rpm

Table 4-4 Summary of morphology

	600 rpm	1000 rpm	2000 rpm	3000 rpm	4000 rpm
Roughness (nm)	3.791	2.816	1.983	1.487	1.313
Z range (nm)	37.906	23.776	21.533	13.159	13.234
Mobility (cm^2/Vs)	0.0040	0.0034	0.0008	0.0006	0.0003

Fig. 4-13 shows the morphology of different solvent used to solve P3HT, o-DCB and chloroform, respectively. The two devices were modified with SAMs of OTS at the gate insulator. We see flatter films in the devices coated with the P3HT / chloroform system. That the boiling point of chloroform is low causes the high evaporation rate of the solvent. The solvent annealing that lowering the evaporation rate has more time for P3HT to self-organize. Thus there are less self-organized P3HT structures in Fig. 4-13 (b) than in Fig. 4-13 (a). It is consistent with the difference of mobility.

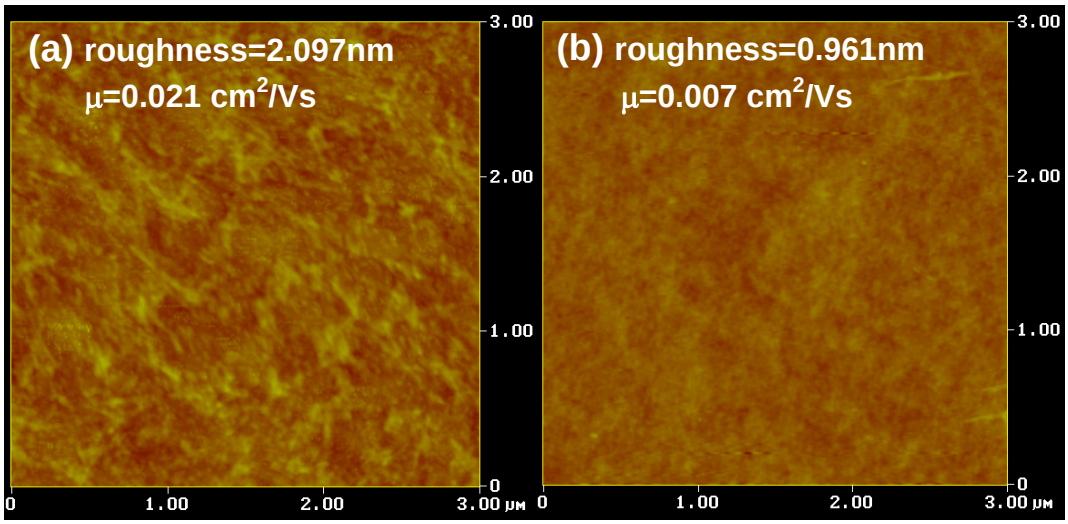

Fig. 4-13 The morphology of different solvent of P3HT (a) o-DCB (b) P3HT

In summary, it was observed that the annealing effect (include the thermal annealing and the solvent annealing) resulted in higher mobilities and had rougher surface morphology. There is a positive relationship between the mobility and the roughness. The reasonable guess is that the self-organization of P3HT cause the high mobility and the rougher surface morphology at the same time. The solvent annealing is capable to extend the drying time of solvent. The P3HT would form regional microcrystalline structures during the solvent evaporation. The structures finally results in the mobility increment and contribute to the rougher surface morphology.

4.2.2 The XRD Diagram of the Different Evaporation Rates

In order to verify the effect of the solvent annealing, the devices with three different evaporation rates were investigated. For the devices of the fastest evaporation rate of the solution, we immediately placed the devices onto the pre-heated hotplate which the temperature was set to 110 ℃ after spin coating. Due to the assistance of the heating, the solvent was dry within 10 seconds. We fabricated the devices with normal evaporation rate by placing the spin coated devices in a glove box and waited until the solvent dried. It took within 1 minute for the solvent dried off. The devices with the slowest evaporation rate were placed into small Petri dishes to decrease the evaporation rate of the solvent. The drying time of the solvent took more than 5 minutes. All samples were thermal annealed at 110 ℃ for 15 minutes to avoid the factor of the thermal annealing.

To reveal the orientation of the different plane in the P3HT films, we used X-ray diffraction (XRD) to acquire the P3HT microstructure. Fig. 4-14 shows the results of the XRD. Fig. 4-14 (a) presents the XRD intensity in linear scale to identify the difference of the strong peaks. In contrary, Fig. 4-14 (b) presents the XRD intensity in logarithmic scale to distinguish the difference of the weak peaks. The thin line of the slow solvent annealing

means the devices placed in the Petri dishes, the thicker line of the rapid solvent annealing means the devices placed in the glow box, and the thickest line of the no solvent annealing means the devices placed in the hotplate immediately after spin coating.

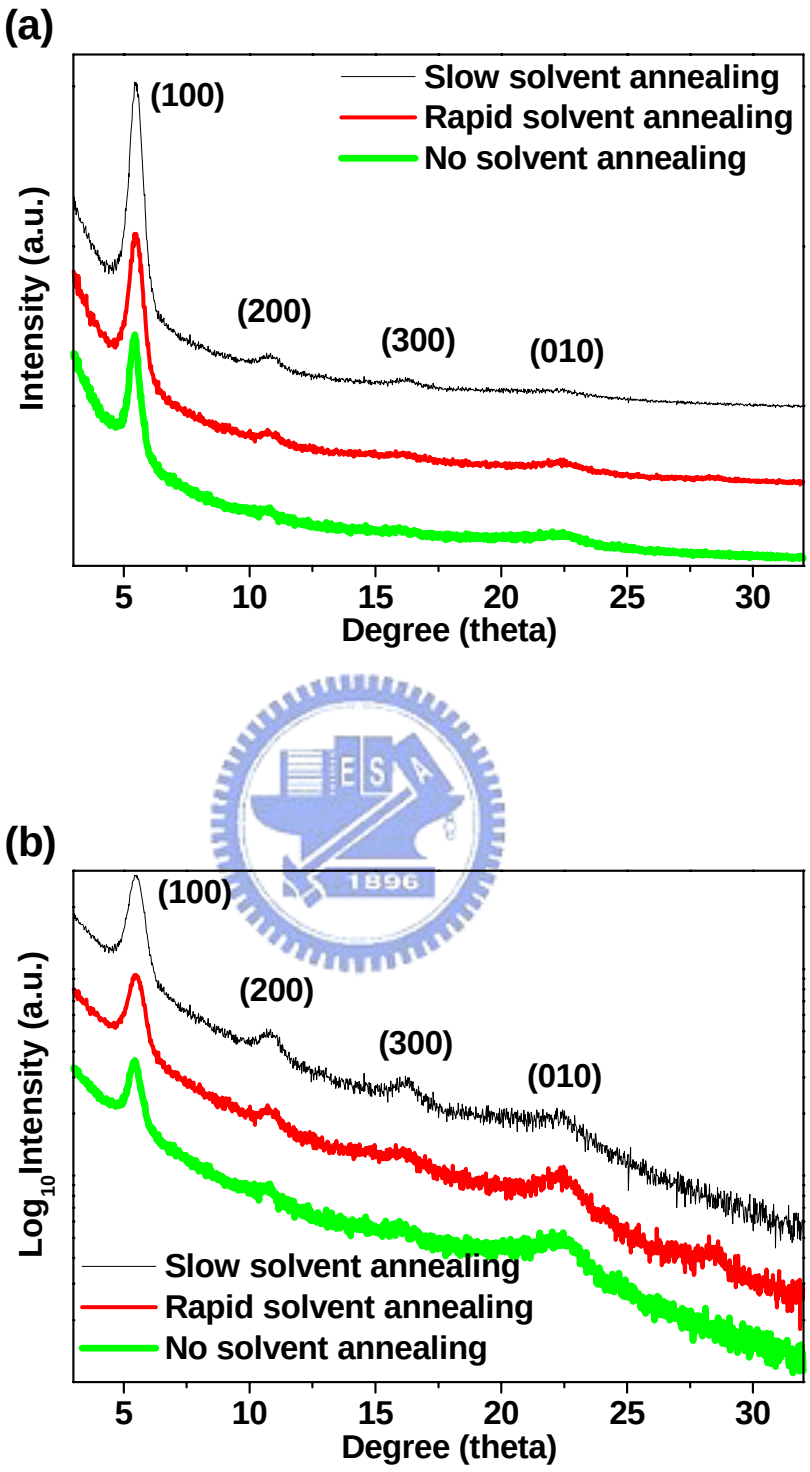

Fig. 4-14 The X-ray diffraction of the different evaporation rates (a) the intensity is in the linear scale (b) the intensity is in the logarithmic scale

Observing the peak of (100) plane, the highest peak is the devices with the solvent annealing treatment and the lowest peak is the devices with the fastest evaporation rate. The intensity of the peak of the (100)-plane increases with the time of the evaporation rates.

Table 4-5 shows the fitting results fitted by the following equation about (100) peaks.

$$y = y_0 + Ae^{-2\left(\frac{x - x_0}{w}\right)^2}$$

Table 4-5 The fittings of (100) peaks

	A	x_0 (θ)	w (θ)	FWHM (θ)
Slow solvent annealing	2803.4	5.478	0.480	0.565
Fast solvent annealing	1679.5	5.468	0.466	0.549
No solvent annealing	1336.9	5.414	0.353	0.416

That the (100) peak of the slow solvent annealing has highest intensity implies that the P3HT lamellae are preferentially aligned in the direction normal to the substrates during solvent annealing. This result is consistent with the changes of the mobility. The mobility would increase with solvent annealing treatment that is mentioned in Chapter 4.1.1. While the solvent evaporates into the environment, the self-organized P3HT lamellae would form amorphous films that are partially ordered microcrystalline. [10] As mentioned in Chapter 1.3, the P3HT lamellae tend to be in the plane that are normal to the substrates if it takes more time to form films. Because the π-π stacking is perpendicular to the main chain of P3HT, the directions of π-π stacking are parallel to the substrates when the P3HT lamellae are normal to the substrates. The structure results in higher mobilities of the devices. Thus, the conclusion is that the slower the evaporation rates are, the more the P3HT lamellae are aligned in the (100)-plane and would result in high mobility.

In Fig. 4-14 (b), it is clear that the (010) peak of the no solvent annealing condition is stronger than any other conditions, and the (010) peak of the slow solvent annealing condition is weakest. The order of the (010) peak intensity is in reverse order of the (100) peak intensity. This phenomena indicates that when more P3HT lamellae align along the (010) plane, there are less P3HT lamellae aligning along the (100) plane due to the planes of (100) and (010) being orthogonal.

We conclude that the orientations of P3HT lamellae have significant effect on the transportation of charge carriers. The solvent annealing can assist the P3HT lamellae to align in the (100) plane not the (010) plane. This would result that the planes of π-π stacking are parallel to the accumulation layers in the channel. Because the charge carrier transportation in P3HT is limited by π-π interchain, the plane of the π-π stacking parallel to the accumulation layers would increase the mobility of the TFT devices.

4.2.3 The UV-Visible Absorption Spectrum

We conclude that the solvent annealing can changes the orientation of P3HT lamellae by XRD. Next, we want to check the relation between the annealing effect and the crystallinity P3HT. P3HT had been coated on transparent glasses to measure the absorption of P3HT. Fig. 4-15 shows the absorption of P3HT in the visible light segment. In order to observe the changes of peaks, all data are normalized.

The fast sol. ann. condition in Fig. 4-15 means the fast solvent annealing that the devices were dried under the glow box filled with nitrogen. The slow sol. ann. means the slow solvent annealing that the devices were dried in the Petri dishes. The solvent of fast solvent annealed devices was dried off within the 1 minute. The evaporation rate of slow solvent annealed devices was slower and needed more than 5 minutes to complete dry off. The thermal annealed devices were annealed at 110 ℃ for 15 minutes.

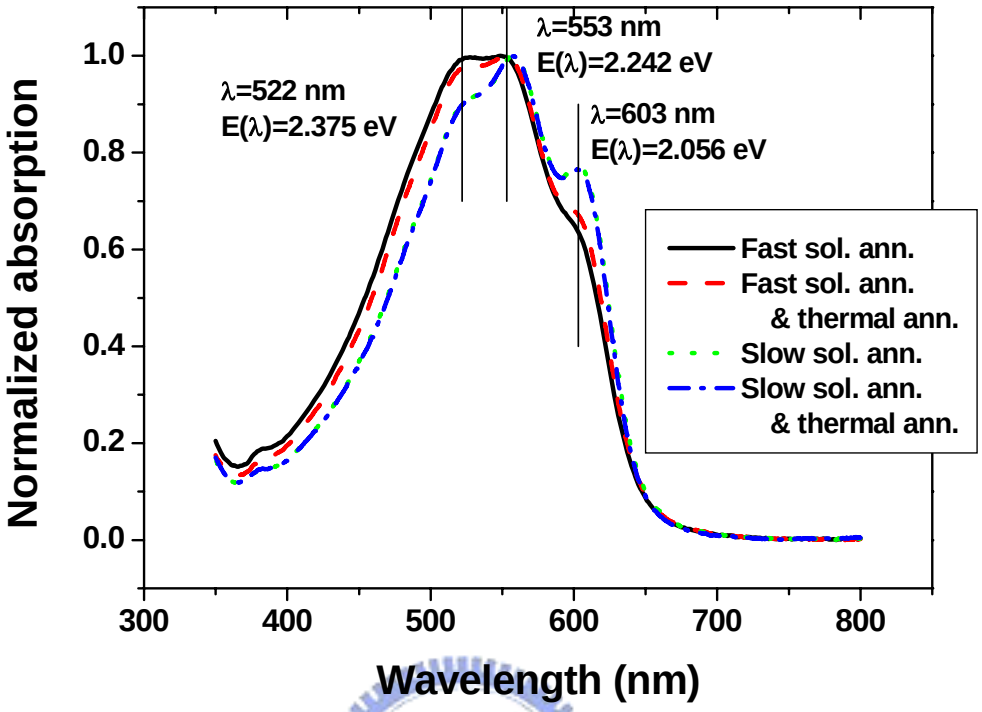

Fig. 4-15 The normalized absorption of the different annealing conditions

The normalized absorption is shown in Fig. 4-15. The normalized absorption spectrum of slow solvent annealed devices almost coincides with the slow solvent annealed and thermal annealed devices. The absorption increased with the slower evaporation time in the shoulder of λ = 603 nm. Under the same evaporation time of the fast solvent annealed devices, the thermal annealing can improve the shoulder slightly.

Observing the peaks at λ = 522 nm and λ = 553 nm, the absorption of the two peaks in the fast solvent annealed devices is nearly the same. In the slow solvent annealed devices condition, the absorption peak of λ = 553 nm is much stronger than the absorption peak of λ = 522 nm. It means that the absorption of the devices with slower evaporation rate have increment at the peak of λ = 553 nm.

The absorption of P3HT films would increase due to the high order and crystallinity.

[26] With high degree ordering P3HT films, there are less disordered films blocking the vibronic absorption of photons. The devices with solvent annealing have more time to form films. The self-organization of P3HT spent more time becoming more regular formations. The spectrum of fast solvent annealed devices has weakest absorption peaks. After thermal annealing, the absorption peaks were strengthen slightly. It indicates that the thermal annealing assists the chain become freer, the films would tend to reach the thermodynamically stable point and form more regular films. The solvent annealed devices have the strongest absorption peaks because of the highest ordering that is enhanced by the slow evaporation rate. In summary, the slow evaporation rate causes the occurrence of the self-organization of P3HT. Consequently, the shoulders at some wavelengths would strengthen due to the increment of the P3HT ordering. Hence the mobility of P3HT-based TFT can be improved.

Chapter 5

Conclusions

From the measurement of the electrical transfer characteristics of thin-film transistors, the annealing effects in the field-effect mobility enhancement has been investigated. The annealing effects in this article are distinguished into two types. One is the traditional thermal annealing. The thermal annealing help the P3HT active layer to reach the thermodynamically stable status with thermal energy. It can result in a more regular arrangement, thereby increase of the mobility. Another is the solvent annealing. The solvent annealing forms a regular P3HT active layer films by lowering the evaporation rate of solvent after spin coating. Due to the self-organization of P3HT, the solvent annealing can assist the P3HT to form regional ordered microcrystalline structures and improve the mobility. The two annealing effects are not exclusive. By combining the solvent annealing and the thermal annealing, the mobility can be improved furthermore.

We obtained the morphology information by AFM. According to the relationship between the roughness and the mobility, we infer the structure of self-organized P3HT cause the changes in morphology and mobility. The P3HT active layer films were examined by XRD to confirm the orientations of P3HT lamellae. The results indicate that the P3HT lamellae tend to align in the plane normal to the substrate if the solvent annealing is applied. The transistors have higher mobility when the P3HT lamellae are align in the plane that is perpendicular to the substrate. Then the absorption of the P3HT films is tested to realize the crystalline structure of P3HT. The absorption spectra indicate that the solvent annealing increases the microcrystalline structure, and enhanced the absorption at shoulders.

As a result, we concluded that the solvent annealing improves the mobility by extend the time of the self-organization of P3HT. Better self-organized P3HT films have improved semiconducting properties and are suitable to be the active layer of transistors.

References

[1] S. R. Forrest, "The path to ubiquitous and low-cost organic electronic appliances on plastic," Nature **428** (6986), 911-918 (2004).

[2] F. Ebisawa, T. Kurokawa, and S. Nara, "Electrical-Properties Of Polyacetylene Polysiloxane Interface," Journal Of Applied Physics **54** (6), 3255-3259 (1983).

[3] A. Tsumura, H. Koezuka, and T. Ando, "Macromolecular Electronic Device - Field-Effect Transistor With A Polythiophene Thin-Film," Applied Physics Letters **49** (18), 1210-1212 (1986).

[4] A. Assadi, C. Svensson, M. Willander et al., "Field-Effect Mobility Of Poly(3-Hexylthiophene)," Applied Physics Letters **53** (3), 195-197 (1988).

[5] G. Horowitz, X. Z. Peng, D. Fichou et al., "Role Of The Semiconductor Insulator Interface In The Characteristics Of Pi-Conjugated-Oligomer-Based Thin-Film Transistors," Synth. Met. **51** (1-3), 419-424 (1992).

[6] C. D. Dimitrakopoulos and P. R. L. Malenfant, "Organic thin film transistors for large area electronics," Adv. Mater. **14** (2), 99-+ (2002).

[7] C. K. Chiang, C. R. Fincher, Y. W. Park et al., "Electrical-Conductivity In Doped Polyacetylene," Phys. Rev. Lett. **39** (17), 1098-1101 (1977).

[8] Z. Bao, A. Dodabalapur, and A. J. Lovinger, "Soluble and processable regioregular poly(3-hexylthiophene) for thin film field-effect transistor applications with high mobility," Applied Physics Letters **69** (26), 4108-4110 (1996).

[9] M. Surin, P. Leclere, R. Lazzaroni et al., "Relationship between the microscopic morphology and the charge transport properties in poly(3-hexylthiophene) field-effect transistors," Journal Of Applied Physics **100** (3) (2006).

[10] H. Sirringhaus, P. J. Brown, R. H. Friend et al., "Two-dimensional charge transport in self-organized, high-mobility conjugated polymers," Nature **401** (6754), 685-688 (1999).

[11] H. Sirringhaus, N. Tessler, and R. H. Friend, "Integrated optoelectronic devices based on conjugated polymers," Science **280** (5370), 1741-1744 (1998).

[12] H. Sirringhaus, P. J. Brown, R. H. Friend et al., "Microstructure-mobility correlation in self-organised, conjugated polymer field-effect transistors," Synth. Met. **111**, 129-132 (2000).

[13] Y. Kim, S. Cook, S. M. Tuladhar et al., "A strong regioregularity effect in self-organizing conjugated polymer films and high-efficiency polythiophene: fullerene solar cells," Nat. Mater. **5** (3), 197-203 (2006).

[14] A. Zen, J. Pflaum, S. Hirschmann et al., "Effect of molecular weight and annealing of poly (3-hexylthiophene)s on the performance of organic field-effect transistors,"

Adv. Funct. Mater. **14** (8), 757-764 (2004).

[15] R. J. Kline and M. D. McGehee, "Morphology and charge transport in conjugated polymer," Polym. Rev. **46** (1), 27-45 (2006).

[16] J. Paloheimo, H. Stubb, P. Ylilahti et al., "Field-Effect Conduction In Polyalkylthiophenes," Synth. Met. **41** (1-2), 563-566 (1991).

[17] A. Babel and S. A. Jenekhe, "Alkyl chain length dependence of the field-effect carrier mobility in regioregular poly(3-alkylthiophene)s," Synth. Met. **148** (2), 169-173 (2005).

[18] H. C. Yang, T. J. Shin, L. Yang et al., "Effect of mesoscale crystalline structure on the field-effect mobility of regioregular poly(3-hexyl thiophene) in thin-film transistors," Adv. Funct. Mater. **15** (4), 671-676 (2005).

[19] J. F. Chang, B. Q. Sun, D. W. Breiby et al., "Enhanced mobility of poly(3-hexylthiophene) transistors by spin-coating from high-boiling-point solvents," Chem. Mat. **16** (23), 4772-4776 (2004).

[20] D. H. Kim, Y. D. Park, Y. S. Jang et al., "Enhancement of field-effect mobility due to surface-mediated molecular ordering in regioregular polythiophene thin film transistors," Adv. Funct. Mater. **15** (1), 77-82 (2005).

[21] D. H. Kim, Y. Jang, Y. D. Park et al., "Surface-induced conformational changes in poly(3-hexylthiophene) monolayer films," Langmuir **21** (8), 3203-3206 (2005).

[22] R. J. Kline, M. D. McGehee, and M. F. Toney, "Highly oriented crystals at the buried interface in polythiophene thin-film transistors," Nat. Mater. **5** (3), 222-228 (2006).

[23] A. Salleo, M. L. Chabinyc, M. S. Yang et al., "Polymer thin-film transistors with chemically modified dielectric interfaces," Applied Physics Letters **81** (23), 4383-4385 (2002).

[24] S. Cho, K. Lee, J. Yuen et al., "Thermal annealing-induced enhancement of the field-effect mobility of regioregular poly(3-hexylthiophene) films," Journal Of Applied Physics **100** (11) (2006).

[25] V. Shrotriya, Y. Yao, G. Li et al., "Effect of self-organization in polymer/fullerene bulk heterojunctions on solar cell performance," Applied Physics Letters **89** (6) (2006).

[26] G. Li, V. Shrotriya, J. S. Huang et al., "High-efficiency solution processable polymer photovoltaic cells by self-organization of polymer blends," Nat. Mater. **4** (11), 864-868 (2005).

[27] D. H. Kim, Y. Jang, Y. D. Park et al., "Controlled one-dimensional nanostructures in poly(3-hexylthiophene) thin film for high-performance organic field-effect transistors," J. Phys. Chem. B **110** (32), 15763-15768 (2006).

[28] J. Park, S. Lee, and H. H. Lee, "High-mobility polymer thin-film transistors fabricated by solvent-assisted drop-casting," Org. Electron. **7** (5), 256-260 (2006).

[29] K. C. Dickey, J. E. Anthony, and Y. L. Loo, "Improving organic thin-film transistor

performance through solvent-vapor annealing of solution-processable triethylsilylethynyl anthradithiophene," Adv. Mater. **18** (13), 1721-+ (2006).

30 Morrison and body, Organic Chemistry, sixth edition, 502 (1992).

31 G. Horowitz, "Organic field-effect transistors," Adv. Mater. **10** (5), 365-377 (1998).

32 P. G. Lecomber and W. E. Spear, "Electronic Transport In Amorphous Silicon Films," Phys. Rev. Lett. **25** (8), 509-& (1970).